A MAGYAR TUDOMÁNYOS AKADÉMIA

MŰSZAKI FIZIKAI KUTATÓ INTÉZETÉNEK

KÖZLEMÉNYEI

O–13

A MAGYAR TUDOMÁNYOS AKADÉMIA MŰSZAKI FIZIKAI INTÉZETÉNEK
KÖZLEMÉNYEI

RESEARCH INSTITUTE FOR TECHNICAL PHYSICS OF THE HUNGARIAN
ACADEMY OF SCIENCES
COMMUNIQUÉ

0 - 13.

Some Reports of the Scientific Staff of the Research Institute for Technical Physics of the Hungarian Academy of Sciences

1974.

A Magyar Tudományos Akadémia Műszaki Fizikai
Kutató Intézete
Budapest, Ujpest 1. Pf. 76.

ИНСТИТУТ ТЕХНИЧЕСКОЙ ФИЗИКИ
ВЕНГЕРСКИЙ АКАДЕМИИ НАУК

Research Institute for Technical Physics
of the Hungarian Academy of sciences

Felelős kiadó: Szigeti György akadémikus, igazgató
Műszaki szerkesztő: Gomperz Istvánné

74-610 "Tempó" F.v.: Szerencsi Sándor
150 példány

CONTENTS

ON THE VECTORIAL REPRESENTATION OF BASIC COLOUR-PERCEPTION AND ITS USE IN COLOUR-MEASUREMENT

G.Lux[x] - J.Schanda

1. Introduction

It is usual to distinguish between two levels of colorimetry, a basic one, where Grassmann's laws are valid and an advanced, perceptual one. In this paper we will stay within the boundaries of basic colorimetry, where linear metrics can be applied. Within these limits it is usual to define three primary colours and use the laws of additive colour mixture to express the problems of tristimulus colorimetry.

In the following an alternative interpretation of this system, based on vector calculus, will be given, and applied to discuss tristimulus colorimetry.

2. Colour transformations

The colour $\underline{S}$[xx] of an unknown spectral distribution can be expressed as the additive sum of three reference stimuli ($\underline{R}$, $\underline{G}$, $\underline{B}$):

$$\underline{S} = R\underline{R} + G\underline{G} + B\underline{B} \qquad 1$$

where R, G and B are the tristimulus values.

Using this equation for all the monochromatic radiations finaly the spectral tristimulus values (STV) $\bar{r}(\lambda)$, $\bar{g}(\lambda)$, $\bar{b}(\lambda)$ are reached, by the help of which the tristimulus values of a colour can be calculated if the spectral distribution

[x] Now with Tungsram Inc.Lamp Works, Budapest.

[xx] Colours are represented by underlined capital letters.

$\underline{S}_\lambda$ of the radiation representing the colour is known:

$$R = \int_{380}^{780} S_\lambda \bar{r}(\lambda)\,d\lambda, \quad G = \int_{380}^{780} S_\lambda \bar{g}(\lambda)\,d\lambda, \quad B = \int_{380}^{780} S_\lambda \bar{b}(\lambda)\,d\lambda \qquad 2$$

The STV-s are characteristic to the $\underline{R}$, $\underline{G}$, $\underline{B}$ reference stimuli, but not to their spectral distribution, as the same colour can be produced by different spectral distributions (metamerism).

It is well known that the same colour matching equation as seen in Equ.1 can be written for other reference stimuli, thus e.g.:

$$\underline{S} = F\underline{F} + H\underline{H} + N\underline{N} \qquad 3$$

Here again equations of the form of Equ.2 hold, only the STV functions ($\bar{f}(\lambda)$, $\bar{h}(\lambda)$, $\bar{n}(\lambda)$) have to be determined.

Equations coupling the two systems of reference stimuli are

$$\begin{aligned} \underline{F} &= R_f \underline{R} + G_f \underline{G} + B_f \underline{B} \\ \underline{H} &= R_h \underline{R} + G_h \underline{G} + B_h \underline{B} \\ \underline{N} &= R_n \underline{R} + G_n \underline{G} + B_n \underline{B} \end{aligned} \qquad 4$$

The tristimulus values expressing the colour attributes of colour $\underline{S}$ in the two systems (Equ.1 and 3.) are coupled by similar equations. Writing the tristimulus values as column vectors it can be shown that equation

$$\begin{bmatrix} F \\ H \\ N \end{bmatrix} = \begin{bmatrix} R_f & R_h & R_n \\ G_f & G_h & G_n \\ B_f & B_h & B_n \end{bmatrix}^{-1} \begin{bmatrix} R \\ G \\ B \end{bmatrix} \qquad 5$$

holds. By denoting the inverse of the matrix in this equation by $\underline{\underline{L}}$ this can be written in a simpler form:

$$\begin{bmatrix} F \\ H \\ N \end{bmatrix} = \underline{\underline{L}} \begin{bmatrix} R \\ G \\ B \end{bmatrix} \qquad 6$$

Using the form of Equ.2. this can be rewritten as

$$\begin{bmatrix} \int_{380}^{780} S_\lambda \, \bar{f}(\lambda)\, dx \\ \int_{380}^{780} S_\lambda \, \bar{h}(\lambda)\, d\lambda \\ \int_{380}^{780} S_\lambda \, \bar{n}(\lambda)\, d\lambda \end{bmatrix} = \underline{\underline{L}} \cdot \begin{bmatrix} \int_{380}^{780} S_\lambda \, \bar{r}(\lambda)\, d\lambda \\ \int_{380}^{780} S_\lambda \, \bar{g}(\lambda)\, d\lambda \\ \int_{380}^{780} S_\lambda \, \bar{b}(\lambda)\, d\lambda \end{bmatrix} \qquad 7$$

This equation has to hold for every S_λ distribution, thus

$$\begin{bmatrix} \bar{f}(\lambda) \\ \bar{h}(\lambda) \\ \bar{n}(\lambda) \end{bmatrix} = \underline{\underline{L}} \cdot \begin{bmatrix} \bar{r}(\lambda) \\ \bar{g}(\lambda) \\ \bar{b}(\lambda) \end{bmatrix} \qquad 8$$

gives the transformation equations for the STV-s. It is very important to notice that $\underline{\underline{L}}$ is independent of λ, and the equations have to hold for every wavelength.

It is well known that the CIE fixed in 1933 the STV-s of the so called average observer, and fixed also a linear transformation of these, a transformation where all the STV-s are non-negative numbers. It is usual to denote this system of STV-s by $\bar{x}(\lambda)$, $\bar{y}(\lambda)$, $\bar{z}(\lambda)$ (CIE-STV-s).

A tristimulus colorimeter should show sensitivity distributions in accordance to these CIE-STV-s. If, however, the instrumental STV-s are a linear transformation of the CIE ones, i.e.

$$\left[\bar{a}_i(\lambda)\right] = \underline{\underline{L}} \left[\bar{x}_j(\lambda)\right], \text{ (with } i=1\ldots4,\ j=1\ldots3) \qquad 9$$

where $\bar{a}_i(\lambda)$ represents the instrumental STV-s (it is usual to use four detectors, thus $i = 1\ldots4$), and $\bar{x}_1(\lambda) = \bar{x}(\lambda)$, $\bar{x}_2(\lambda) = \bar{y}(\lambda)$ and $\bar{x}_3(\lambda) = \bar{z}(\lambda)$, an exact colour measurement is still possible.

In practice it is usual to set $\underline{\underline{L}}$ in Equ.9. as a unity matrix (using the $\bar{a}_i(\lambda)$ curves instead of the $\bar{x}_i(\lambda)$ ones), but even in the more general case of an arbitrary matrix $\underline{\underline{L}}$ Equ.9. does not hold for every wavelength in question (380 nm $\leq \lambda \leq$ 780 nm) exactly. This leads to measurement errors. Budinszky [1] showed a method of finding an optimal $\underline{\underline{L}}$ matrix based on a minimum calculus.

In the following we shall discuss a vector representation of the spectral power distributions and show how vector calculus can be applied to describe colorimetry. By the help of this we shall get an answer on the problem of optimal transformation as well.

3. Vectorial representation of colour measurement

As well known the human eye can distinguish between spectral distributions only in the form of integrals. All the different P_λ spectral distributions that yield the same

$$X = \int_{380}^{780} P_\lambda \bar{x}(\lambda)\,d\lambda, \quad Y = \int_{380}^{780} P_\lambda \bar{y}(\lambda)\,d\lambda, \quad Z = \int_{380}^{780} P_\lambda \bar{z}(\lambda)\,d\lambda \qquad 10$$

tristimulus values are metameric, we cannot distinguish them.

In Equ.5. we used already the column vector representation of the tristimulus values. Using the system of the reference stimuli as basic vectors the manyfold of colours can be represented as the elements of this tridimensional space, where the tristimulus values give the coordinates of the colour-vector.

It is straight-forward to regard the spectral power distributions as elements of a multidimensional vector space [2-4]. It can be shown that in such a representation all the laws of vector calculus hold. The only exception would be the multiplication by a negative number, as this operation would lead out of the set of spectral distributions. If, however, the system of spectral distributions is completed with these "virtual" distributions, in a similar way as the concept of virtual colours is used, this problem is solved without any difficulty. Thus all the continuous or quadraticly integrable functions are

elements of this vector space. The number of dimensions of this space can be reached by finding a basis. Such a basis could be the system of the sine or cosine functions used in the Fourier-series of the functions. From this it can be seen that our vector space is countably infinite.

It can be shown that inner products between the elements of this linear space can be defined in the following form:

f (x) function is represented by vector $\underline{f}$

g (x) function is represented by vector $\underline{g}$

and

$$\int f(x)\, g(x)\, dx = c \text{ (real)} \longrightarrow \underline{f} \cdot \underline{g} = c \qquad 11$$

As both the P_λ power distributions and the $\bar{x}_i$ ($\bar{x}_1 = \bar{x}(\lambda)$, $\bar{x}_2 = \bar{y}(\lambda)$, $\bar{x}_3 = \bar{z}(\lambda)$) STV functions can be represented in this vector space by vectors ($\bar{P}$ and $\bar{x}_i$), the colour measurement is, according to Equ.11., just the inner product of the $\bar{P}$ vector and the $\bar{x}_i$ spectral tristimulus vector.

4. Vectorial picture of colour vision

The spectral power distribution of a given colour gives a vector $\underset{\sim}{P}^x$ in the space of power distributions. In the same space the STV-s of the CIE-system ($\bar{x}(\lambda)$, $\bar{y}(\lambda)$, $\bar{z}(\lambda)$) are represented by three vectors: $\underline{x}_1$, $\underline{x}_2$ and $\underline{x}_3$. These vectors form a threedimensional subspace; in the following we will refere to this subspace as to the colour measuring subspace.

The visual perception of a spectral power distribution is the orthogonal projection of this power distribution vector into the colour-measuring subspace. The colour perception is influenced only by this projection and not by the "arbitrarily" chosen triplet of STV-s, forming a basis of the subspace. The projection can be expressed as the linear combination of the reference stimuli vectors $\underline{x}_i$, ($i = 1 \ldots 3$), but just as well in an orthonormal system of basic vectors (see e.g. 3), reached as linear transformation of the reference stimuli vectors $\underline{x}_i$ ($i = 1 \ldots 3$). Budinszky [1] used in his calculation an orthonormal system $\underline{k}_i$ ($i = 1 \ldots 3$) where

$$\underline{k}_i \, \underline{k}_j = \delta_{ij} \begin{cases} = 0, & \text{if } i \neq j \\ = 1, & \text{if } i = j \end{cases} \qquad i, j = 1 \ldots 3 \qquad 12$$

(We will come back to this problem in Chapter 6.)

Let us try to find that particular basis, where the tristimulus values are coordinates of the projection.

It can be shown that every spectral power distribution vector has one and only one projection in the colour-measuring subspace. The projection of $\underset{\sim}{P}^x$ will be marked by P_o. The tristimulus values of the spectral power distribution $\underset{\sim}{P}^x$ are the $\underset{\sim}{P}^x \underline{x}_1$, $\underset{\sim}{P}^x \underline{x}_2$, $\underset{\sim}{P}^x \underline{x}_3$ inner products. We will show now that the $P^x \underline{x}_i$ ($i = 1,2,3$) tristimulus values are the coordinates in the inverted system of $\underline{x}_i$ ($i = 1 \ldots 3$) : $\underline{y}_i$ ($i = 1 \ldots 3$), where $\underline{y}_i \, \underline{x}_j = \delta_{ij}$ see Equ.12., i.e.:

$$\sum_{i=1}^{3} \left(\underset{\sim}{P}^x \underline{x}_i \right) \underline{y}_i = \underline{P}_o, \qquad \text{where } \underline{y}_i \, \underline{x}_j = \delta_{ij} \qquad 13$$

Let us describe P_o in the system of y_i ($i = 1 \ldots 3$) in the following way

$$\underline{P}_o = r_1 \underline{y}_1 + r_2 \underline{y}_2 + r_3 \underline{y}_3 \qquad 14$$

As $\underline{P}_o$ is the projection of $\underset{\sim}{P}^x$,

$$\underset{\sim}{P}^x \underline{x}_i = \underline{P}_o \, \underline{x}_i , \quad i = 1 \ldots 3 \qquad 15$$

and thus

$$\sum_{i=1}^{3} (\underset{\sim}{P}^x \underline{x}_i) \underline{y}_i = \sum_{i=1}^{3} (\underline{P}_o \, \underline{x}_i) \underline{y}_i = \sum_{i=1}^{3} (r_1 \underline{y}_1 \underline{x}_i + r_2 \underline{y}_2 \underline{x}_i + r_3 \underline{y}_3 \underline{x}_i) \underline{y}_i$$

and this, by using 13 and 14, gives:

$$\sum_{i=1}^{3} (\underset{\sim}{P}^x \underline{x}_i) \underline{y}_i = \sum_{i=1}^{3} r_i \underline{y}_i = \underline{P}_o \qquad 16$$

Thus we reached the very simple result that for all those spectral power distributions for which P_o is the projection (i.e. for all the colours metameric with P_o), the STV-s represent the projection as coordinates in the invert system of basic vectors.

By the help of these results we get a somewhat better insight into the colour vision and measurement mechanism. Postulating the spectral power distribution space, and the colour measuring subspace, the Grassmann laws are reached very easily:

According to the first Grassmann law, in case of additive colour mixture, the final colour depends only on the colour and not on the spectral distribution of the primeries. As the spectral power distribution and colour measuring spaces are linear, and vector addition corresponds to additive colour mixture, just the projections of the spectral distributions into the colour measuring subspace show these characteristics. Grassmann's second law (the necessity of three independent data to describe a colour) shows that the colour measuring subspace is three-dimensional.

Grassmann's third law that the colour mixing series are continuous is a consequence of the linearity of the vector spaces.

Most important among these is the first Grassmann law, describing metamerism. In vector representation this means that an (infinite) number of spectral distributions can have the same projection in the colour measuring subspace. Fig. 1. visualizes this in a simplified form: $\vec{x_1}$ and $\vec{x_2}$ represent the basis of the colour measuring subspace (let us take it now as only two-dimensional) and $\vec{e}$ the other n-2 coordinates ($n \to \infty$) of the spectral power distribution space. $\vec{P^x}$ is a vector in this space, and $\vec{P_o}$ is its projection in the subspace. At the same time $\vec{P^x_{met}}$ is an other spectral distribution yielding $\vec{P_o}$ as projection, i.e. the same colour, thus $\vec{P^x}$ and $\vec{P^x_{met}}$ represent metameric colours.

This gives a - theoretical - tool for finding a basis of the colour measuring subspace. It is necessary to determine a high number of pairs of spectral

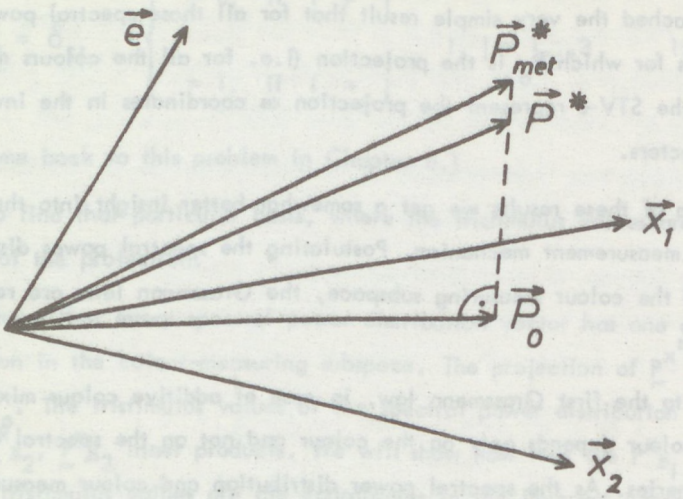

Fig. 1. Schematic representation of the spectral power distribution and colour measuring spaces, and the colour measurement of two metameric colour stimuli ($\vec{P}^{x}$ and $\vec{P}^{x}_{met}$).

distributions being metameric. If one calculates the difference of every two distributions forming a pair this difference vectors form a subspace, and the colour measuring subspace contains the vectors perpendicular to these difference vectors.

By the help of this experiment it is thus possible to determine the colour measuring subspace. The $\underline{x}_i$ STV-s (i.e. the $\bar{x}(\lambda)$, $\bar{y}(\lambda)$, $\bar{z}(\lambda)$ functions) are a basis of this space, determined by the help of some further requirements: One of the basic vectors should coincide with the $V(\lambda)$luminosity curve, all the coordinates of the vectors forming the basis should be non-negative, and the vector, representing the equienergetic spectrum should be of equal distance from the basis. These demands determine the CIE STV-s unambiguously, and by this we can reach these distributions - theoretically - without using the concept of primary colours.

5. The transformation of an instrumental system

Tristimulus values of colours can be determined either by measuring the spectral power distribution P_λ and using the equations of Equ.10., or by duplicating the STV functions by detector - filter combinations and thus performing the integrations of Equ.10. in the detectors themselves. In practice the filter-detector combinations never match the STV functions perfectly, and thus a transformation of the instrumental results into the CIE tristimulus values might increase the measuring accuracy.

From the discussions in Chapter 3 and 4 it is obvious that an exact transformation is possible only if the instrumental STV "vectors" lie within the subspace spanned by the CIE STV vectors $\underline{x}_1$, $\underline{x}_2$, $\underline{x}_3$.

The instrumental subspace is not necessarily threedimensional (this depends on the number of detectors used, in usual tristimulus colorimeters it is four dimensional, due to the fact that the $\bar{x}(\lambda)$ curve shows two maxima), in the following we will take it as five dimensional giving a further degree of freedom for the construction. Increasing the number of detectors enables a more complete transformation, but the practical circuitry becomes increasingly complicated, five channels seem to be a reasonable compromise. Let us mark these instrumental STV vectors by $\underline{a}_i$ ($i = 1 \ldots 5$).

Measuring $\underset{\sim}{P}^{\times}$ by this instrument yields the $\underset{\sim}{P}^{\times}\,\underline{a}_i$ values as results, i.e. the measurement gives us the projection of $\underset{\sim}{P}^{\times}$ in the subspace spanned by the vectors $\underline{a}_1$, $\underline{a}_2$, $\ldots$ $\underline{a}_5$.

Let us denote the coordinates of this projection by p_i ($i = 1 \ldots 5$), and the projection of $\underset{\sim}{P}^{\times}$ in this subspace by $\underset{\sim}{P}$. Thus

$$\begin{aligned}
\underset{\sim}{P}^{\times}\underline{a}_1 &= \underset{\sim}{P}\underline{a}_1 = (p_1\underline{a}_1 + p_2\underline{a}_2 + p_3\underline{a}_3 + p_4\underline{a}_4 + p_5\underline{a}_5)\,\underline{a}_1 \\
\underset{\sim}{P}^{\times}\underline{a}_2 &= \underset{\sim}{P}\underline{a}_2 = (p_1\underline{a}_1 + p_2\underline{a}_2 + p_3\underline{a}_3 + p_4\underline{a}_4 + p_5\underline{a}_5)\,\underline{a}_2 \qquad 17 \\
\underset{\sim}{P}^{\times}\underline{a}_5 &= \underset{\sim}{P}\underline{a}_5 = (p_1\underline{a}_1 + p_2\underline{a}_2 + p_3\underline{a}_3 + p_4\underline{a}_4 + p_5\underline{a}_5)\,\underline{a}_5
\end{aligned}$$

Performing the multiplication and using a column vector notation for p_i ($i = 1 \ldots 5$): $\vec{p}$, writing also the five results of the measurement ($\underset{\sim}{P}\underline{a}_i$ ($i = 1 \ldots 5$)) in this form: $\vec{P}$; and realizing that the $\underline{a}_i\underline{a}_k$ products form the a_{ik} elements of a matrix $\underline{\underline{A}}$, Equ.17. can be written in a simpler form:

$$\vec{P} = \underline{\underline{A}}\ \vec{p} \qquad 18$$

and thus the coordinates are given by

$$\vec{p} = \underline{\underline{A}}^{-1}\ \vec{P} \qquad 19$$

$\vec{P}$ is the "instrumental value", the tristimulus values can be calculated from this in the following way:

The instrument produces the $\underset{\sim}{P} = \sum_{i=1}^{5} p_i\underline{a}_i$ vector, and the tristimulus values are the

$$\underset{\sim}{P}\,\underline{x}_1,\quad \underset{\sim}{P}\,\underline{x}_2,\quad \underset{\sim}{P}\,\underline{x}_3 \quad \text{products.}$$

Thus e.g.

$$\underset{\sim}{P}\underline{x}_1 = (p_1\underline{a}_1 + p_2\underline{a}_2 + p_3\underline{a}_3 + p_4\underline{a}_4 + p_5\underline{a}_5)\,\underline{x}_i =$$

$$= p_1\underline{a}_1\underline{x}_1 + p_2\underline{a}_2\underline{x}_2 + \ldots + p_5\underline{a}_5\underline{x}_5 \qquad 20$$

Using again the column vector and for the $\underline{x}_i\,\underline{a}_k$ product the m_{ik} matrix element notation, the tristimulus values ($\vec{X}$) are:

$$\vec{X} = \underline{\underline{M}}\ \vec{P} \qquad 21$$

where m_{ik} is an element of matrix $\underline{\underline{M}}$.

By the help of Equ.19. this gives

$$\vec{X} = \underline{\underline{M}}\ \underline{\underline{A}}^{-1}\ \vec{P} \qquad 22$$

Thus matrix $\underline{\underline{M}}\ \underline{\underline{A}}^{-1}$ gives the final transformation. To visualize this, Fig. 2 shows an oversimplified version of the measurement: $\vec{P}^{x}$ is the spectral power distribution in the total spectral power distribution space, consisting of the

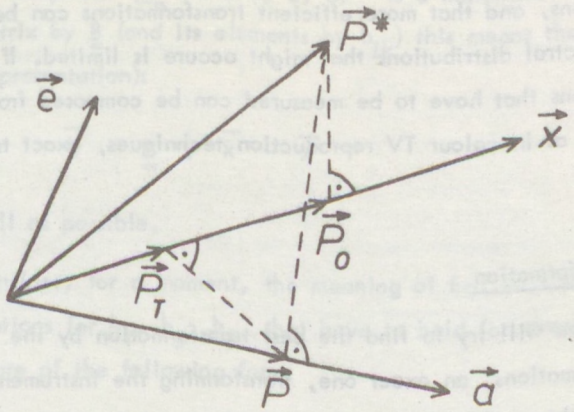

Fig.2. Schematic representation of the spectral power distribution, colour measuring and instrumental subspaces, showing an ideal and an instrumental measurement together with a transformation ($\vec{P}^{\vec{x}} \rightarrow \vec{P}_o$ and $\vec{P}^{\vec{x}} \rightarrow \vec{P} \rightarrow \vec{P}_T$)

independent instrumental subspace $(\vec{a})$, the colour measuring subspace $(\vec{x})$ and the $N - N_a - N_x$ dimensional space (here N_a and N_x represents the number of dimensions of the instrumental and colour measuring subspace) visualized by vector $\vec{e}$.

A correct colour measurement projects $\vec{P}^{\vec{x}}$ onto the $\vec{x}$ axis and yields thus the colour $\vec{P}_o$. The instrument performs instead of this the projection onto axis $\vec{a}$, resulting in the "instrumental value" $\vec{P}$, the transformation according to Equ.21. performs the projection onto the $\vec{x}$ axis giving the final value $\vec{P}_T$.

The aim of the transformation technique is to decrease the average $\left|\underline{P}_T - \underline{P}_o\right|$ value. It will be shown in the next Chapter that the method outlined above gives the "best" transformation for all the monochromatic colours. As normal colours are composed by monochromatic radiations the transformation will give better tristimulus values also for most of the practical colours. It is, however, quite obvious that it might deteriorate the measurement results of some special

spectral distributions, and that more efficient transformations can be found, if the number of spectral distributions that might occure is limited. If, e.g. the spectral distributions that have to be measured can be composed from three basic distributions as in colour TV reproduction techniques, exact transformations can be found.

6. Optimal transformation

In the following we will try to find the best transformation by the help of two successive transformations, an exact one, transforming the instrumental STV vectors into an orthogonal system, and a second one giving the smallest mean error in transforming all the monochromatic radiations.

Let us denote the instrumental basis by $\underline{a}_i$ ($i = 1 \ldots 5$) and the orthogonal ones by $\underline{k}_i$ ($i = 1 \ldots 5$). Due to orthogonality

$$\underline{k}_i \, \underline{k}_j = \delta_{ij} \qquad 23$$

where δ_{ij} is the Kronecker-symbol (see Equ.12.).

Using the column vector representation the transforming matrix ($\underline{\underline{0}}$) between $\underline{a}_i$ and $\underline{k}_m$ ($i, m = 1 \ldots 5$) is found from the following equation:

$$\underline{\underline{0}} \cdot \vec{a} = \vec{k} \qquad 24$$

Thus, if the elements of matrix $\underline{\underline{0}}$ are denoted by σ_{ik}, it can be written that

$$\underline{k}_i = \sum_{k=1}^{5} \sigma_{ik} \, \underline{a}_k \quad (i = 1 \ldots 5) \qquad 25$$

Putting Equ.25. into Equ.23., and taking into consideration that multiplication is commutative, 15 equations can be found for the 25 elements of the matrix. The other elements can be chosen arbitrarily. Thus it is always possible to use instead of the instrumental functions an orthogonal transformation of these.

The problem is now to find such a transformation matrix that the difference between the transformed orthogonal instrumental vectors and the basis of the

colour measuring subspace ($\underline{x}_n$ (n = 1, 2, 3) is a minimum.
Denoting this matrix by $\underline{\underline{B}}$ (and its elements by b_{ik}) this means that (by using column vector representation):

$$\vec{h} = \underline{\underline{B}} \cdot \vec{k} - \vec{x} \qquad 26$$

should be as small as possible.

(Let us now reconsider, for a moment, the meaning of Equ.26.: It covers really three equations for $\underline{h}_1$, $\underline{h}_2$, $\underline{h}_3$, that have to hold for every (wavelength) dimension, thus are of the following form:

$$h_1(\lambda) = [b_{11}\, k_1(\lambda) + b_{12}\, k_2(\lambda) + .. + b_{15}\, k_5(\lambda)] - \bar{x}(\lambda) \qquad 27$$

and similarly for $\bar{y}(\lambda)$ and $\bar{z}(\lambda)$ with $h_2(\lambda)$, $h_3(\lambda)$ and $b_{21} \ldots b_{35}$.)

Instead of finding the minimum of Equ.26. it is reasonable to look for the minimum of

$$H_i = \left| \underline{h}_1 \right|^2 \qquad (i = 1, 2, 3) \qquad 28$$

the norm of vector $\underline{h}_i$, this is, due to Equ.11. an other description of

$$H_i = \int_{380}^{780} [h_i(\lambda)]^2 d\lambda \quad (i = 1, 2, 3) \qquad 29$$

The minimum requirements are of the following form:

$$\frac{\partial H_i(b_{11}, b_{12}, \ldots, b_{15})}{\partial b_{12}} = 0 \qquad 30$$

Writing Equ. 27. and 29. into Equ.30., and by using the orthogonality criterium of Equ.23. we get that the matrix elements of $\underline{\underline{B}}$ have to be of the following form

$$b_{ik} = \underline{x}_i \, \underline{k}_k \qquad 31$$

Comparing Equ.31. with Equ.21. and 22. it is seen that matrix $\underline{\underline{M}}$ is equal to matrix $\underline{\underline{B}}$, if the instrumental system is orthogonal; and thus in the vector transformation technique of Chapter 5 matrix $\underline{\underline{A}}$ constructed from the instrumental STV vectors has the same meaning as the transformation of the instrumental STV vectors into an orthogonal basic vector system.

Thus the transformation equation of Equ.22. yields the "best" transformation of the instrumental subspace into the colour measuring one. (Matrix $\underline{\underline{M}}$ performs a rotation within the instrumental subspace giving the "best" threedimensional subspace.)

7. Application of the matrix transformation technique

The above described technique has been used to correct some crude photocell-filter combinations. In each combination a red sensitive Si-photoelement and two colour filters have been used. We calculated the difference between the uncorrected instrumental STV functions and the CIE STV functions, as well as the same values using the transformed STV-s, always correcting the absolute values of the curves to give the same area under the curve, and calculated the mean deviations.

Table I and II show some representative results of this calculation. As seen from Table II although filter combination No.2 is better than combination No.3, the transformed results of combination 3 are the best ones. This means that it is possible to find a combined optimum for filter thickness and transformation.

Table I.

Filter combinations used

	combination 1	combination 2	combination 3
$\underline{a}_1$:	BG 18 + OG 1	BG 18 + GG 20	BG 18 + GG 20
$\underline{a}_2$:	BG 18 + BG 3	BG 18 + BG 1	BG 18 + BG 3
$\underline{a}_3$:	BG 18 + VG 4	BG 18 + VG 4	BG 18 + GG 10
$\underline{a}_4$:	BG 18 + BG 24	BG 18 + BG 24	BG 18 + BG 24

Table II.

Filter combination	Instrumental-CIE STV-s			Transformed-CIE STV-s			Mean deviation from CIE values	
	x	y	z	x	y	z	instum.	transf.
1	1,427	0,244	0,731	1,294	0,175	0,565	0,541	0,474
2	0,944	0,244	0,731	0,887	0,103	0,706	0,399	0,382
3	0,968	0,463	0,731	0,925	0,268	0,561	0,439	0,372

the values in column 2-7 are calculated as $\sqrt{\sum_{i=1}^{n}\left[\bar{a}_{jq}(\lambda_i) - \bar{x}_j(\lambda_i)\right]^2}$

where $\bar{a}_{jq}$ refers to the instrumental STV-s, $\bar{x}_j$ to the CIE ones (j: x, y, z; q = 0 for the instrumental and is t for the transformed one).

Table III gives, as an example, the values of the transformation matrix for combination 3.

Table III.

Transformation matrix of filter combination No.3

0,966	0,834	0,092	0,029
-0,193	0,308	1,134	-0,043
0,0374	-2,103	-0,042	1,393

Fig. 3 shows the spectral distribution of the instrumental, the transformed and the CIE $\bar{y}(\lambda)$ curve. It is seen that the transformation improves the curve form considerably.

Our aim is to use the matrix transformation technique in a tristimulus light source colorimeter, thus we calculated the chromaticity coordinates for several light sources as well Fig. 4. and 5, shows the spectral distribution of some sources used in this calculation, Table IV-VI presents the chromaticity coordinates of these sources for the instrumental, the transformed and the CIE STV-s (column A, B and C) as well as differences between the instrumental and CIE, as well as the transformed and CIE chromaticity coordinates (column D

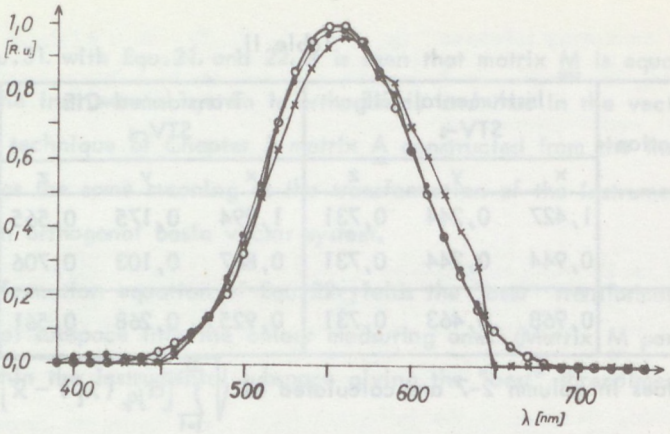

Fig.3. A realized $\bar{y}(\lambda)$curve: —×—×— The transformed $\vec{y}_t(\lambda)$ curve: —●—●— and the CIE one: —○—○—

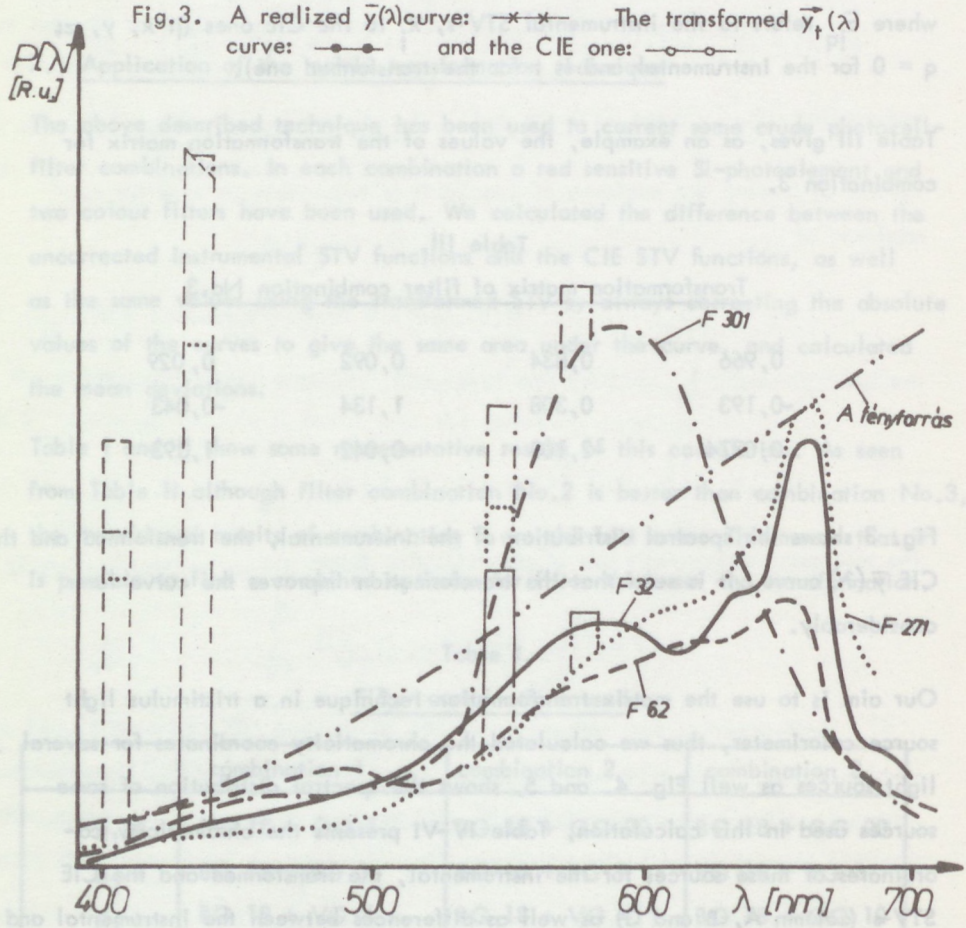

Fig. 4. Some spectral power distributions used in the calculations

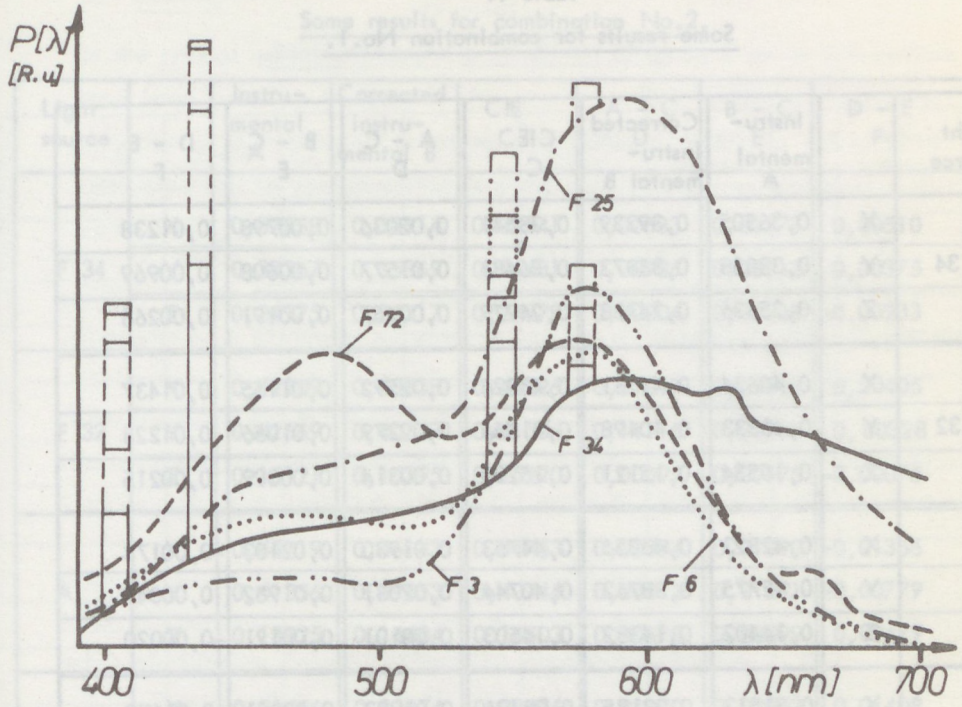

Fig. 5. Some spectral power distributions used in the calculations

and E). The difference of column D and E visulaizes the amount of amelioration (column F). For every filter combination the mean relative amelioration (F_{mean}/D_{mean}) has been calculated as well. It is interesting to note that for the relatively bad combination No.1 a strong amelioration was achieved, the relatively good combination No.2 is not much better after transformation as combination No.1, on the other hand combination No.3 shows a mean amelioration comparable to that of combination No.1, and gives at the same time relatively good results.

The instrumental realization of these results is under way, together with the development of a new computer program enabling the determination of the optimal filter thickness together with the best transformation matrix.

Table IV

Some results for combination No.1.

Light source		Instru-mental A	Corrected instru-mental B	CIE C	A - C D	B - C E	D - E F
F 34	X	0,36505	0,39339	0,38541	0,02036	0,00798	0,01238
	Y	0,38058	0,35873	0,36481	0,01577	0,00608	0,00969
	Z	0,25436	0,24788	0,24979	0,00457	0,00191	0,00266
F 32	X	0,40634	0,44381	0,43226	0,02592	0,01155	0,01437
	Y	0,43833	0,40498	0,41554	0,02279	0,01056	0,01223
	Z	0,15534	0,15121	0,15220	0,00314	0,00099	0,00215
A	X	0,42823	0,46856	0,44753	0,01930	0,02103	-0,00173
	Y	0,42775	0,38762	0,40744	0,02031	0,01982	0,00049
	Z	0,14402	0,14382	0,14503	0,00101	0,00121	-0,00020
F 6	X	0,31513	0,33185	0,33436	0,01923	0,00251	0,01672
	Y	0,36326	0,35568	0,35373	0,00953	0,00195	0,00758
	Z	0,32161	0,31247	0,31191	0,00970	0,00056	0,00914
F 25	X	0,37345	0,40352	0,40807	0,03462	0,00455	0,03007
	Y	0,41555	0,39115	0,38820	0,02735	0,00295	0,02440
	Z	0,21100	0,20534	0,20373	0,00727	0,00161	0,00566
Mean:					0,01606	0,00635	0,00971

$$\frac{F_{mean}}{D_{mean}} = 0,60$$

Table V

Some results for combination No.2.

Light source		Instru-mental A	Corrected instru-mental B	CIE C	A - C D	B - C E	D - E F
F 34	X	0,37658	0,38914	0,38541	0,00883	0,00373	0,00510
	Y	0,37367	0,35869	0,36481	0,00986	0,00612	0,00375
	Z	0,24975	0,25217	0,24979	0,00004	0,00238	-0,00233
F 32	X	0,42209	0,43838	0,43226	0,01017	0,00612	0,00405
	Y	0,42669	0,40767	0,41554	0,11115	0,00787	0, 00328
	Z	0,15121	0,15395	0,15220	0,00099	0,00175	-0,00076
A	X	0,44719	0,46143	0,44753	0,00034	0,01390	-0,01356
	Y	0,41356	0,49453	0,40744	0,00512	0,01291	-0,00779
	Z	0,13925	0,14404	0,14503	0,00578	0,00099	0,00479
F 6	X	0,31466	0,32874	0,33436	0,01970	0,00562	0,01408
	Y	0,36351	0,35127	0,35373	0,00978	0,00246	0,00731
	Z	0,32183	0,32000	0,31191	0,00992	0,00808	0,00184
F 25	X	0,41149	0,40572	0,40807	0,00342	0,00235	0,00107
	Y	0,39032	0,38701	0,38820	0,00212	0,00119	0,00094
	Z	0,19819	0,20727	0,20373	0,00554	0,00354	0,00200
Mean:					0,00685	0,00527	0,00158

$$\frac{F_{mean}}{D_{mean}} = 0,23$$

Table VI

Some results for combination No.3.

Light source		Instru-mental A	Corrected instru-mental B	CIE C	A - C D	B - C E	D - E F
F 3	X	0,35216	0,37174	0,37838	0,02622	0,00664	0,01958
	Y	0,39146	0,38328	0,37631	0,01516	0,00697	0,00818
	Z	0,25638	0,24498	0,24531	0,01107	0,00033	0,01074
F 62	X	0,35840	0,37580	0,36774	0,00934	0,00806	0,00128
	Y	0,31432	0,30373	0,31043	0,00389	0,00670	-0,00281
	Z	0,32728	0,32048	0,32183	0,00545	0,00135	-0,00410
F 72	X	0,29276	0,30548	0,30288	0,01012	0,00260	0,00752
	Y	0,33212	0,32421	0,32619	0,00593	0,00198	0,00395
	Z	0,37512	0,37031	0,37092	0,00420	0,00061	0,00359
F 271	X	0,42077	0,44352	0,43085	0,01008	0,01267	-0,00259
	Y	0,35955	0,34057	0,35368	0,00587	0,01311	-0,00724
	Z	0,21968	0,21591	0,21547	0,00421	0,00044	0,00377
F 301	X	0,39476	0,41572	0,41997	0,02521	0,00425	0,02096
	Y	0,40150	0,38548	0,38150	0,02000	0,00398	0,01602
	Z	0,20374	0,19880	0,19853	0,00521	0,00027	0,00494
Mean:					0,01080	0,00466	0,00613

$$\frac{F_{mean}}{D_{mean}} = 0,57$$

8. Summary

In the present work the vector representation of spectral power distributions have been used. By the help of this it was possible to give a visual interpretation of such concepts as metamerism, spectral tristimulus values of an instrument and its transformation into the colour measuring subspace, a space corresponding to the human colour vision mechanism.

Transfomation techniques for transforming the spectral sensitivity distribution functions of a tristimulus colorimeter as close as possible to the CIE spectral tristimulus values have been discussed. Possibilities and limitations of this technique are shown theoretically as well as on practical examples. It is possible to achieve a twofold mean amelioration of the experimental results by this technique.

Literature

1. Budinszky, J.: Híradástechnika 21. 110-25. 1971.
2. Shapiro, W.A.: JOSA 56. 795. 1966.
3. Shapiro, W.A.: Optica Acta 19. 235-42. 1972.
4. Schanda, J., Lux, G.: AIC Conference Colour 73.

Table VI.

Light source		[illegible]mental A	instrument B	CIE	A - C	B - C	D - E
	X	0,35216	0,37174	0,37838	0,02622	0,00664	0,01958
F 3	Y	[illegible]	[illegible]	[illegible]	[illegible]	[illegible]	[illegible]
	Z	[illegible]	[illegible]	[illegible]	[illegible]	[illegible]	[illegible]
	X	[illegible]	[illegible]	[illegible]	[illegible]	[illegible]	[illegible]
[illegible]	Y	[illegible]	[illegible]	[illegible]	[illegible]	[illegible]	[illegible]
	Z	0,32728	0,32048	0,32183	0,00545	0,00135	0,00410
	X	0,29276	0,30548	0,30288	0,01012	0,00260	0,00752
F 72	Y	0,33212	0,32421	0,32619	0,00593	0,00198	0,00395
	Z	[illegible]	[illegible]	[illegible]	[illegible]	[illegible]	[illegible]
	X	[illegible]	[illegible]	[illegible]	[illegible]	[illegible]	[illegible]
F 271	Y	[illegible]	[illegible]	[illegible]	[illegible]	[illegible]	[illegible]
	Z	0,21968	0,21591	0,21547	0,00421	0,00044	0,00377
	X	0,39476	0,41572	0,41997	0,02521	0,00425	0,02096
F 301	Y	0,40150	0,38548	0,38150	0,02000	0,00398	0,01602
	Z	0,20374	0,19880	0,19853	0,00521	0,00027	0,00494

Mean: 0,01080 0,00466 0,00613

$$\frac{F_{mean}}{D_{mean}} = 0,57$$

THE TEMPERATURE DEPENDENCE ANALYSIS OF THE CHARGE CARRIER CONCENTRATION IN GaP

Károly Somogyi

Introduction

The majority of the informations characteristic for the various impurities, which are present in a semiconductor may be obtained in the temperature range, where the impurities are not yet fully ionized. Due to their relatively low activation energies this applies generally at low temperatures [1]. One of the most important and directly measurable data in this range is the concentration of the free charge carriers which depends, beside the temperature, on the concentration and the activation energy of the impurities.

The activation energies of the impurities determining generally the type of the conduction are about of 0.04-0.10 eV in GaP, which came into the foreground from the viewpoint of research after the preparation of the first light emitting diodes [2]. This activation energy is high relative to the activation energies found in the usual semiconductors, therefore the impurities are practically not fully ionized even at room temperature. So in the GaP the temperature dependence of the charge carrier concentration may be described well in the range of 77-400 K by the well known formula valid for the ionization of the impurities. In the case of electron conduction we have [1]:

$$\frac{n\,(N_A + n)}{N_D - N_A - n} = \frac{1}{g}\, N_c \exp\left(-\frac{E_D}{kT}\right) \qquad (1)$$

where the notations are as follows

n - free charge carrier concentration

N_D - donor concentration

N_A - acceptor concentration

N_C - conduction band state density;

$$N_C = \frac{2\,(2\,\pi\, m^x kT)^{3/2}}{h^3}$$

g - degeneracy factor

E_D - donor activation energy

k - Boltzmann's constant

T - absolute temperature

m^x - effective mass

h - Planck's constant

On the basis of formula (1) the analysis of the temperature dependence permits the determination of the majority and minority impurity concentratirons, the value of the effective mass and the activation energy of the majority impurity. But this analysis is not simple, due to the complexity of formula (1), therefore several methods have been developed for this purpose, the most significant of which is the iteration analysis by the least square method [3], and the fitting along straight line besed on the following form of formula (1) [4]:

$$A = \frac{n\,(N_A + n)}{(N_D - N_A - n)N_c'} = \frac{1}{g}\left[\frac{m^x}{m_o}\right]^{3/2} \exp\left(-\frac{E_D}{kT}\right) \qquad (2)$$

where $N_c' = N_c (m^x)^{-3/2}$.

The right side of this equation versus $1/T$ is a straight line in a semi-log plot. With this mode of expressing the temperature dependence of the charge carrier concentration by representing the left side of the equation as versus $1/T$ a straight line must be obtained, as well. For obtaining the straight line N_A and N_D, as the free parameters of the left side, must be varied. The slope of the obtained straight line gives the activation energy, and the value A

extrapolated on the temperature $1/T = 0$ gives the quotient $(m^x)^{3/2} g^{-1}$. The advantage of the method is that only two parameters must be varied for obtaining the values of all four (and eventually five) fitting parameters.

The parameters determined with the help of formula (1), and in the first place the effective mass, show a wide scatter for GaP, according to literature. (See e.g. ref. [5], where the value of the product $(m^x)^{3/2} \cdot g^{-1}$ varies between 0.19 - 2.7, however, g may be assumed as constant.) Such a wide scatter of the value of m^x cannot be explained by the possible temperature dependence, or charge carrier concentration dependence of the effective mass, but may be assumed sooner to be the error of the analysis. This assumption made the examination of the analysability of formula (1), of the applicability of the Hutson method and the reliability of the results necessary [6].

Analysis by the Hutson method

Fig. 1 shows some typical results of the temperature dependence of the charge carrier concentration measured in p-GaP doped with Zn. But for controlling

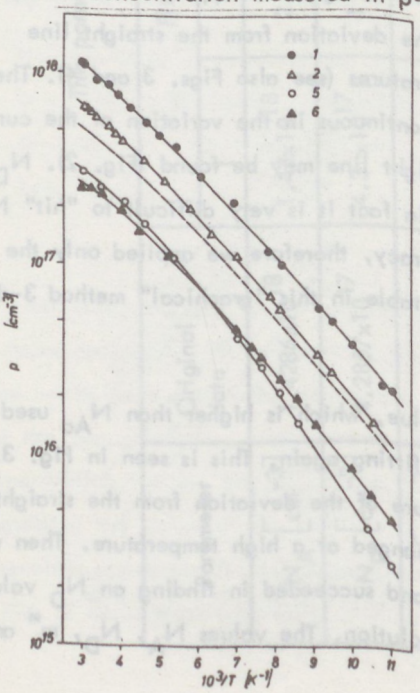

Fig. 1. Typical temperature dependence of the carrier concentration in p-GaP. Continous lines are experimental curves, the dashed line is the calculated curve, which was taken for the analysis.

the method we did not rely on the measurement's results, as the value of the measurement error would have disturbed the cleannes of the examination greatly; instead we have choosen assumed N_{Ao}, N_{Do}, m^*_o and E_{Ao}.

parameters, which are characteristic in the GaP. Fig. 1. shows the concentration calculated by formula (1) with these parameters in dashed line. (The similarity of the calculated and the measured curves is seen well.) The accuracy of the concentrations determined in this way is 0.01 % at least. These parameters are given in Table I. In the following we have carried out the analysis of the calculated concentration data by the Hutson method, with selecting N_D to a freely assumed N_A value for the fitting, while leaving N_A constant. (As the formulae 1 and 2 apply with due interpretation to both the electrons and the holes, so for the analysis it is indifferent, whether an n-type, or a p-type material is examined and the subsequent results apply also to both cases. Important was only that the calculated $p(T^{-1})$ curve should be characteristic for the real GaP crystals, so in the following the notations applied for type p material are used).

The variation of the curve form of the realtionship (2) in the course of the variation of N_D, when N_{Ao} was chosen for the value of N_A, is shown in Fig. 2a. By Fig. 2 it is seen that when $N_D < N_{Do}$ was chosen for the purpose of fitting, the deviation from the straight line appears in the first place down. When $N_D > N_{Do}$, then the deviation from the straight line appears preferentially up at high temperatures (see also Figs. 3 and 4). The transition between these deviations is continuous in the variation of the curve and in this course also the required straight line may be found (Fig. 2). N_D approximates N_{Do} closely. (Naturally in fact it is very difficult to "hit" N_{Ao} given preliminarily with a 5-digit accuracy, therefore we applied only the value of N_A with the practically selectable in this "graphical" method 3-digit accuracy.)

In the following we assumed an N_A value, which is higher than N_{Ao} used in calculating the curve and tried the fitting again. This is seen in Fig. 3. N_D was increased from 0 until the nature of the deviation from the straight line, similarly to the previous case, changed at a high temperature. Then we looked for the intermediate N_D value and succeeded in finding an N_D value producing the straight line giving the solution. The values N_A, N_D, m^* and

Table I.

The parameter sets for several cases.

Parameter	Original data	Fitted parameters Number of sets				
		1	2	3	4	5
N_A $[cm^{-3}]$	1.4286×10^{18}	1.43×10^{18}	2.00×10^{18}	8.00×10^{17}	1.60×10^{18}	1.00×10^{18}
N_D $[cm^{-3}]$	4.2857×10^{17}	4.3×10^{17}	1.09×10^{18}	1.25×10^{16}	6.38×10^{17}	5.50×10^{16}
E_A [meV]	37.3	37.8	34.6	67.4	36.1	54.9
m^x $[m_o]$	0,400	0.404	0.628	0.823	0.4975	0.4975

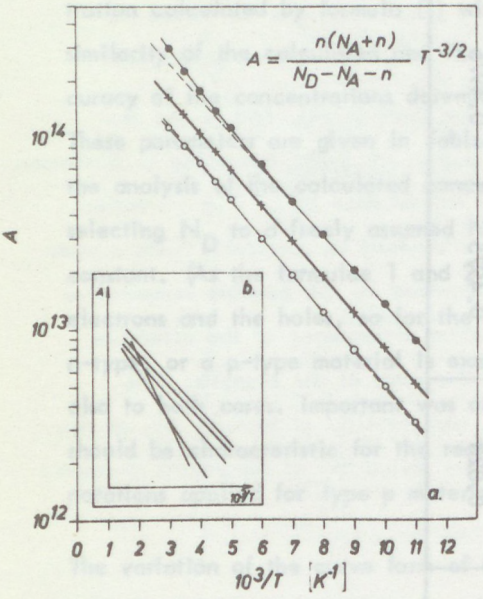

Fig. 2.

a) The change of the curve form, the deviations from the straight line by $N_A \approx N_{Ao}$. $N_A = 1.43\times10^{18}$ cm^{-3}; $N_D = 0\text{-}3\times10^{17}$; x-4.3x $\times10^{17}$ and ●-6x10^{17} cm^{-3}

b) The position of the five fitted straight lines relative to each other

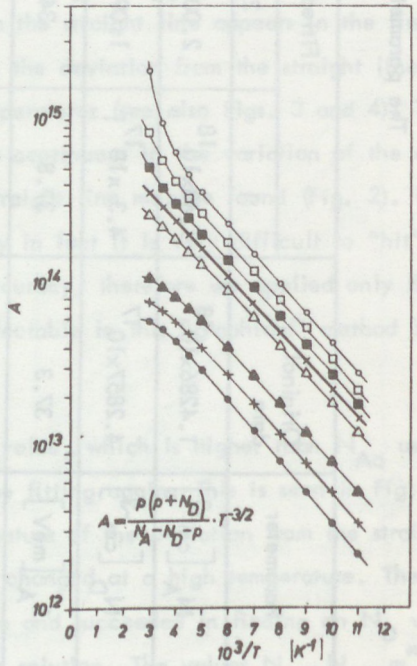

Fig. 3. The change of the curve form by $N_A > N_{Ao}$.

$N_A = 2\times10^{18}$ cm^{-3}; N_D = o -1.4x10^{18}; □ -1.3x10^{18}; ■ -1.2x10^{18}, x-1.09x10^{18}, Δ -1x10^{18}, ▲ -6x10^{17}, + - 4.3x10^{17} and ● - 3x10^{17} cm^{-3}.

E_A belonging to this N_D value and differing, naturally, from N_{Ao}, N_{Do}, m^*_o and E_{Ao} are also given in Table I.

We have also assumed additional arbitray N_A values partly higher and partly lower (Fig. 4) than N_{Ao} and as expected on the basis of Figs. 2-3; in every case an N_D supplying the straight line could be found. The position of these straight lines is shown in Fig. 2b and the data of the parameter sets are given in Table I. Self-evidently the produced parameter sets are totally different and not all of them can be correct. From Table I. it is seen that each set of the parameters is completely realistic, contain data which are existent in the GaP and cannot be distinguished on the basis of their reality.

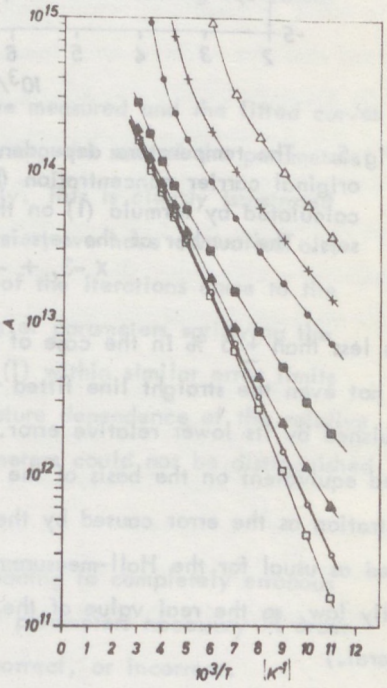

Fig. 4. The change of curve form by $N_A < N_{Ao}$. $N_A = 8\times10^{17}\,cm^{-3}$, $N_D = \Delta\ 6\times10^{17}$, $+\ 4.3\times10^{17}$, $\bullet\ 3\times10^{17}$, $\blacksquare\ 1\times10^{17}$, $\blacktriangle\ 3\times10^{16}$, $o\ 1{,}25\times10^{16}$, $\square$ -from 0 up to $1\times10^{15}\,cm^{-3}$.

For controlling the sets of the parameters and for findig their errors respectively we have calculated the temperature dependence of the charge carrier concentration with each set of the parameters by expression (1). Experience has shown that the concentrations calculated in this way approximated well the original concentration values. For indicating the accuracy of the agreement we have calculated the value of the relative errors assigned to the individual sets of the parameters appearing in the concentration versus the temperature. This is shown in Fig. 5 demonstrating clearly that in the studied temperature range the relative

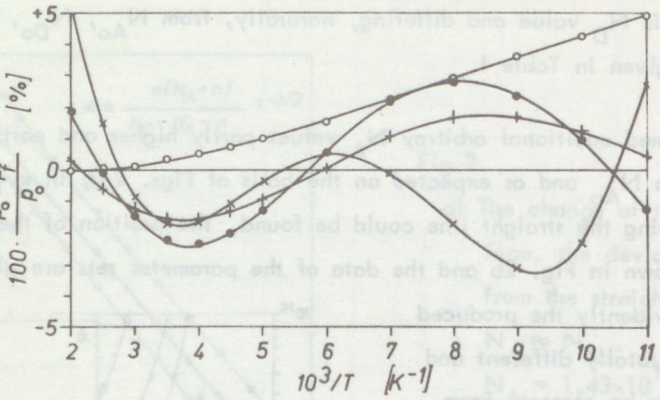

Fig.5. The temperature dependence of the relativ error. p_o is the original carrier concentration (Fig.2.), p_f is the concentration calculated by formula (1) on the basis of the fitted parameter sets. The number of the sets is given in Table I, O -1, ● -2, x -3, + -4.

error is less than ± 5 % in the case of each set of the parameters and with this regard not even the straight line fitted with the original N_{Ao} value can be distinguished by its lower relative error. Each set of the parameters may be regarded equivalent on the basis of the relative errors obtained in carrer [illegible] concentration as the error caused by them is considerably less than the ± 10 % accepted as usual for the Hall-measurements. (In the GaP the Hall voltage is generally low, so the real value of the error is in fact not les than ± 10 % in general.)

The continuity of the error curves shown in Fig. 5 is due to the fact that because of the calculation of the initial "experimental curve" the "measurement error of the concentration" is 0.01 %; if real measurement results were fitted in a similar way, then instead of the continuous curves we would find a statistical error scattering surpassing ± 5 % and by this the difference of the sets of the parameters would be still less evaluable.

It may be assumed that when this method is used for fitting, then after the first good fit (whereby the first straight line could be obtained) the determined set of the parameters would be accepted as correct, which is not always true un-

conditionally, on the basis of the above said. This might be the reason why e.g. in. ref. [5] extreme m^* values are found.

On the basis of the recalculations of carrier concentration and the calculations of the relative errors it must be stated that the selection of the wrong parameters cannot be assigned to the Hutson method, rather it may be assumed that equation (1) may be solved for several sets of parameters beeing equivalent within certain accuracy limits.

As soon as the (average) difference between the measured and the fitted curves becomes less than the (average) measurement error, the sets of the parameters used for fitting get indistinguishable immediately. This is clearly issustrated in Fig. 5. Accordingly, in a less detailed manner, we have controlled also the least squares method and by the character of the iterations came to the conclusion that also by this method several sets of parameters satisfying the measured relationship on the basis of equation (1) within similar error limits can be produced. The character of the temperature dependence of the relative error shows also that the obtained sets of parameters could not be distinguished by the method of the least squares either.

The possibility of the analysis of formula (1) leading to completely erronous results makes the control of the obtained set of parameters necessary in order to attain information on whether the result is correct, or incorrect.

The selection of a correct set of parameters would be ensured by determining the temperature dependence of the charge carrier concentration over a wider range extending both to higher and lower temperatures. If the state of complete ionization can be attained at high temperatures in the temperature dependence of the concentration, i.e. when $p = N_A - N_D$, then the analysis of the curve based on formula (2) is safe, as the difference of the impurity concentrations can be unequivocally determined and only one data must be varied for obtaining the single straight line. But the experimental results show that in GaP complete ionization cannot be attained even at high temperatures [5], [7], so only as

approximative value for $N_A - N_D$ may be found at the most, facilitating little the safe determination of the parameters. The $N_A - N_D$ differences found in Table I correspond to the "experimental curve" plotted in dashed lines in Fig.1. $N_A - N_D$ is nowhere less than the "measured" maximum free charge carrier concentration. In spite of this fact an uncertainty presents itself.

The lower temperature limit for determining the concentration, i.e. its extension to lower temperatures respectively would be just as important. By Fig. 5 it is seen that the relative error increases (fast, according to the calculations) at the boundary of the temperature range and may leave relatively soon the limits of $\pm$ 5 %, which would be characteristic of a bad result. But unfortunately in the GaP this leads frequently to no result either, as under 77 K the variation of the charge carrier concentration and of mobility can not be measured or assumes a character, which cannot be described by formula (1) any more [7]. So the extension of the temperature limits is impossible in the case of the GaP.

The raised problem, as it is seen, is sharpened specifically in the case of the GaP. The fact that the analysis and the determination of the parameter cannot be univocal, might be caused by the narrow temperature range utilizable practically in the case of the GaP. In other materials (e.g. Ge), where no smiliar excluding cause exists neither at low, nor at high temperatures, the correctness of the obtained parameters cannot be doubted on the basis of the above.

The effect of the various parameters on the character of $n(T^{-1})$

A method for controlling the correctness of fitting may be found by using instead of formula (1) a simplified form ot it at low temperatures. With the conditions of

$$n \ll N_A \quad \text{and} \quad n \ll N_D - N_A \tag{3}$$

formula (1) may be written in the following form:

$$n = \frac{N_D - N_A}{N_A} \cdot \frac{N_c}{g} \exp\left(-\frac{E_D}{kT}\right) \qquad (4)$$

On the basis of this form the activation energy can be determined graphically from the slope of the temperature dependence of the charge carrier concentration, if the product $n^{-1}T^{3/2}$ is plotted versus $1/T$.

Partly on the basis of what has been said in the preceding paragraph and partly with respect to meeting the conditions (3) necessary for determining E_D, we have studied the temperature dependence variations of the charge carrier concentration under the influence of the various parameters according to the cases, which may occur in the GaP. Figs. 6, 7, 8 and 9 show several sets of calculated $p(T^{-1})$ curves with varying the individual parameters. It is seen in

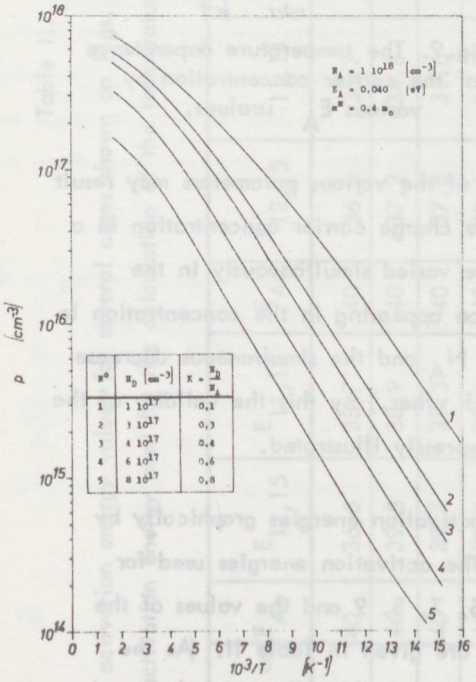

n°	N_D [cm^{-3}]	$K = \frac{N_D}{N_A}$
1	1 10^{17}	0,1
2	3 10^{17}	0,3
3	4 10^{17}	0,4
4	6 10^{17}	0,6
5	8 10^{17}	0,8

Fig.6. The temperature dependence of the carrier concentration by various N_D values.

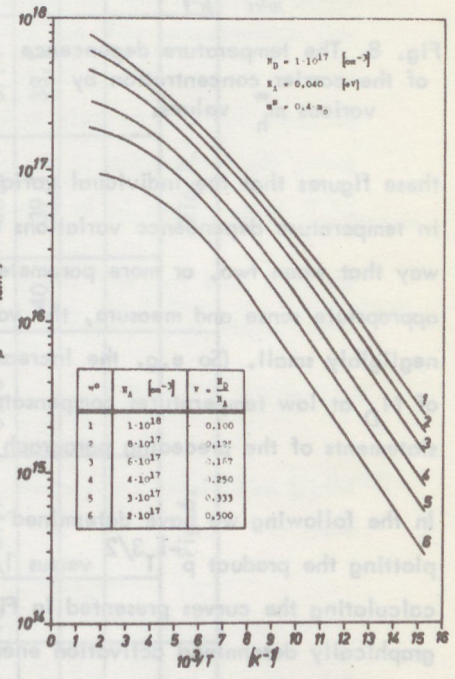

n°	N_A [cm^{-3}]	$r = \frac{N_D}{N_A}$
1	1·10^{18}	0.100
2	8·10^{17}	0.125
3	6·10^{17}	0.167
4	4·10^{17}	0.250
5	3·10^{17}	0.333
6	2·10^{17}	0.500

Fig.7. The temperature dependence of the carrier concentration by various N_A values.

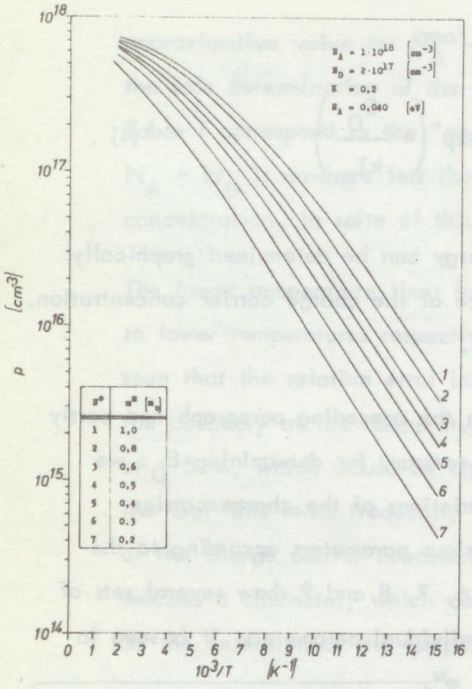

Fig. 8. The temperature depencence of the carrier concentration by various m_h^* values.

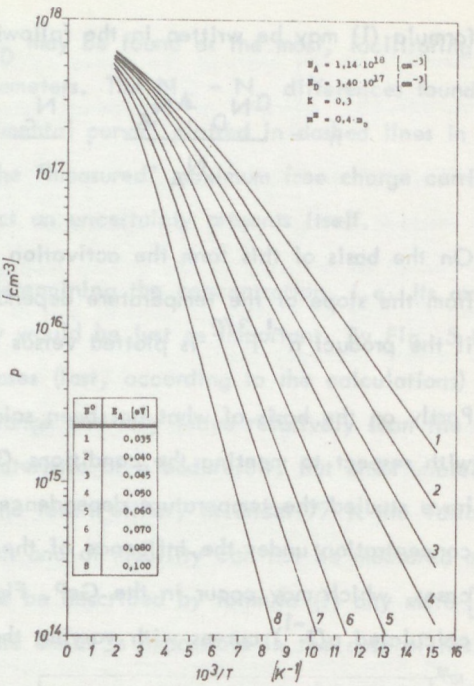

Fig. 9. The temperature dependence of the carrier concentration by various E_A values.

these figures that the individual variations of the various parameters may result in temperature dependence variations of the charge carrier concentration in a way that when two, or more parameters are varied simultaneously in the appropriate sense and measure, the variation appearing in the concentration is negligibly small. (So e.g. the increase of N_A and the simultaneous decrease of N_D at low temperatures compensate each other.) By this the validity of the statements of the preceding paragraph is expressly illustrated.

In the following we have determined the activation energies graphically by plotting the product $p^{-1}T^{3/2}$ versus 1/T. The activation energies used for calculating the curves presented in Figs. 6, 7, 8, 9 and the values of the graphically determined activation energies are given in Table II. (As the "accuracy" of the concentration values in the calculated curves is better than $\pm$ 0.01 %, we have based the graphic determination of E_A always on

Table II.

The activation energy values for several cases shown on Figs. 6, 7, 8, 9 in meV-s. E_{Ao} is the original value of activation energy used for the calculation of the temperature dependence of the carrier concentration.

Curve nimber on Figures	E_{Ao}	$E_{12,15}$	$E_{11,13}$	E_{Ao}	$E_{12,15}$	$E_{11,13}$	E_{Ao}	$E_{12,15}$	$E_{11,13}$	E_{Ao}	$E_{12,15}$	$E_{11,13}$
1	40	36,6	33,7	40	36.6	33.7	40	36.6	33.7	35	34.2	33.4
2	40	39.5	38.9	40	37.2	34.6	40	37.4	34.9	40	39.5	39.0
3	40	39.7	39.3	40	37.8	35.6	40	38.2	36.4	45	44.7	44.4
4	40	39.8	39.6	40	38.4	36.7	40	38.6	37.1	50	49.8	49.6
5	40	39.9	39.8	40	38.8	37.4	40	38.9	37.8	60	59.8	59.8
6				40	39.1	38.1	40	39.3	38.5	70	69.9	69.8
7							40	39.6	39.1	80	79.8	79.8
8										100	99.8	99.8
	Fig.6.			Fig.7.			Fig.8.			Fig.9.		

the concentrations belonging to two temperatures, namely in two cases each.) We have calculated the concentration for the plots up to the temperatures corresponding to $(10^3/T) = 15$, e.i. lower than the boiling point of the liquid N_2, so in one case we have used the concentration corresponding to $10^3/T = 12$ and 15. The value obtained in this way is E_{12-15}. In the other case we used the concentrations corresponding to $10^3/T = 11$ and 13, as basis, which max be regarded more frequent in the measurement range over 77 K and obtained E_{11-13}. It is seen that $E_{11-13} \leqq E_{12-15}$, because over 77 K the conditions (3) are satisfield with a less close approximation. As it can be seen from Table II, the initially fixed E_A values are approximated well by the E_{12-15} values, but an acceptable approximation is ensured also by the E_{11-13} values, especially in the case of high activation energies and a high degree of compensation.

This means that if the activation enegy can be determined according to the conditions (3) in the temperature range used, then the result obtained in this way approximates well the correct activation energy and may be used in the case of the uncertainty in the parameter determination described in the preceding chapter. But unfortunately in part of the cases the low temperature range ensuring the satisfaction of the conditions (3) cannot be reached even down to 77 K (e.g. curves 1. in Figs. 6, 7 and 8).

We must note that the charge carrier concentration range corresponding to the intermediate temperatures existing in principle, where the conditions

$$N_D \gg n \gg N_A \tag{5}$$

would be satisfield and where the activation energy could be determined on the basis of

$$n = \left(\frac{N_D N_c}{g} \right)^{1/2} \exp \left(- \frac{E_D}{2kT} \right) \tag{6}$$

cannot be found in the presented cases. The values of the activation energy based on the assumption (5) does not even approximate those given in Table II, so these values are unusable.

Conclusions

The analysis of the relationship (1) shows that the determination of the parameters N_A and N_D needed especially for the analysis of the low temperature mobilities (the case of scattering on the ionized and the neutral impurities) ^{e} and the determination of the effective mass and the activation energy respectively may be uncertain, possibly reflected in contradictions appearing in the fitting of the temperature dependence of the mobility. The obtained set of the parameters must be controlled in each case and this is only supported partly by the activation energy which can be determined in the low temperature section of the temperature dependence of the charge carrier concentration.

Acknowledgements

Author is very indebted to Mr. B. Pődőr and Mr. J. Balázs for the important discussions and to Mrs. Zs. Puspöki-Fogarasi for the help in computations.

References

1. Smith, R.A.: Semiconductors, Cambridge Univ.Press., 1959.
2. Handbook of Electronic Materials V.2. III-V. Semiconducting Compounds IFI/Plenum N.Y.-W.-L. 1971.
3. Toyama, M.; Unno,K.; Naito, M.: Jap.J. Appl.Phys. 8, (1969) 1118.
4. Hutson.R.A.: Phys. Rev. 108 (1957) 222.
5. Montgomery, H.C.; Feldmann, W.L.: J. Appl. Phys. 36 (1965) 3228.
6. K.Somogyi: te be published
7. Casey, A.C.; Ermanis, F.; Wolfstirn, K.B.: J. Appl. Phys. 40 (1969) 2945.

A SIMPLE NORMAL INCIDENCE MICROREFLECTOMETER ARRANGEMENT

J. Peisner and M. Pintér

Abstract

An inexpensive modification of a normal incidence reflecometer is described which allows absolute measurements of reflectivity and transmission on very small areas (0,2 mm x 0,5 mm) of crystals and thin layers. The horizontal and vertical position of the sample can be adjusted by micrometer screws and is reproducible within ± 0,01 mm. A simple three-mirror system is incorporated allowing easy adaptation to different types of monochromators having different horizontal divergence of the monochromatic beam following the exit slit.

Introduction

It is often desirable to obtain absolute values of the near normal incidence reflectivity on very small areas of crystals or thin films through a large spectral range. Usual equipment requires samples as large as 10-20 mm square. Microspectrophotometers developed for the purposes of biological researches enable only transmission measurements to be made [1].

Several authors refer to microreflection measurements (see Tubbs [2], Fried [3], Knopp [4] and Collins [5]. All these authors use a monochromator or a spectrograph and a microscope as major components. Common disadvantage of this technique is that the reflectivity of the microsample is determined as a relative value compared to a previously calibrated reference sample, without

the possibility of checking the absolute reflectivity of the latter. By applying several modifications to a well-known normal incidence reflectometer arrangement ([6] - [8]), a versatile reflectometer-microreflectometer equipment has been built by us. The apparatus enables the measurement of absolute values for reflectivity and transmission on samples of usual size as well as on microsamples (0,2 mm x 0,5 mm). During "microreflectometer-operation" a quartz microscope objective is inserted in the light path and this focuses the light on the sample. Reflectivity is determined in comparison to the reference surface. Absolute reflectivity of this later is determined in the same apparatus, without the application of the focusing objective ("reflectometer-operation"). The checking of this reflectivity can be quickly repeated.

2. Equipment

The schematic diagram of the apparatus is demonstrated in figure 1. The basic part a normal incidence single mirror reflectometer is very similar to the

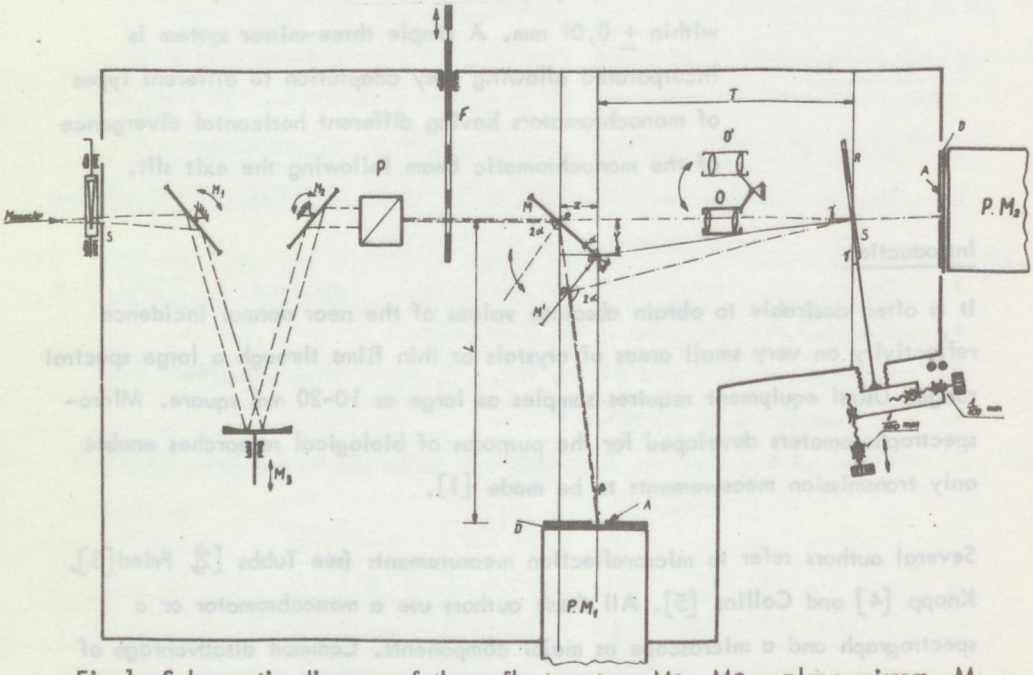

Fig.1. Scheamatic diagram of the reflectometer M_1, M_2 - plane mirrors, M_3 - concave mirror, P - polarizer prism, F - tilter-holder, OM - pivoting plane mirror, Q - microscope objective, S - sample, R - reference mirror, A - apperture, D - light diffuser

equipment reported by EXPOSITO et al[8], but the dimensions are drasticaly changed in order to be able to accomodate the microreflectometer attachment.

The absolute value of the reflectivity of a sample can be directly determined by taking the ratio of the light intensities measured with the PM photomultiplier in position OM and OM of the plane mirror pivoting about axis 0. The microscope objective is now in position Y, and we will call thet "reflectometer-operation" of the apparatus.

The central ray of the light beam satisfies the following relations:

$$\beta = \gamma = 2\alpha - \frac{\pi}{2}$$

$$\operatorname{tg}\beta = \operatorname{tg}\gamma = \frac{z}{L}$$

$$\operatorname{tg}\gamma = \frac{Y}{T}$$

$$\operatorname{tg}\alpha = \frac{z}{Y}$$

We fixed the values of L and γ, and tried to optimize the geometry for the microreflection measurements. The dimensions and angles used in our apparatus are: L=100 mm, $\gamma = 7^{\circ}$, $\alpha = 48{,}5^{\circ}$, T = 88,47 mm, z = 12,28 mm, Y = 10,86 mm.

For obtaining the true value of the absolute reflectivity a parallel monochromatic light beam is necessary. As the light beam leaving the exit slit of a monochromator is divergent, we use a simple mirror system: M_1 and M_2 are plane mirrors which can be rotated and M_3 is a concave mirror capable of beeing translated ant rotated. This system allows easy adaptation of the reflectometer to different monochromators (e.g to the Zeiss SPM 2 or the monochromator part of the SPECTROMOM UV-VIS Spectrometer made by the Hungarian firm MOM).

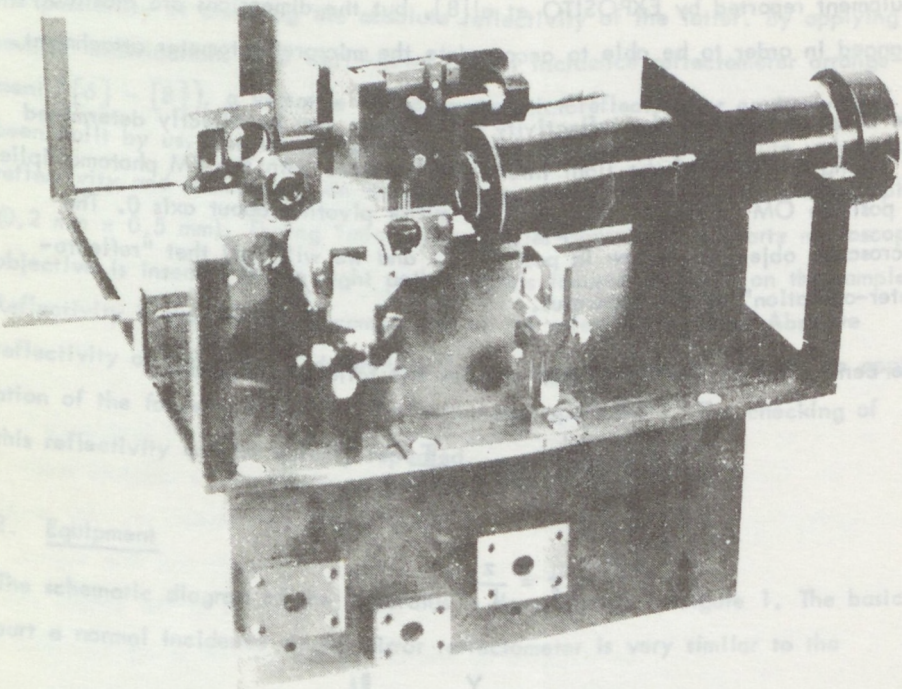

Fig. 2 General view of the set-up

The use of a parallel beam allows a polariser to be included. A Glan air-spaced polariser prism (P) covering a wavelength range from 0,02 μ to 2,5 μ is mounted on a turnable dial, so that it may be easily removed from the light path if not required.

A three position filter holder (F) can be optionally employed for transmission measurement on normal size solid or liquid samples in cuvette-holders.

By applying a quartz microscope objective in position Q and pivoting the plane mirror into position OM , we can detect the light reflected from very small areas approximately 0,3 mm^2. The horizontal and vertical positions of the samples may be adjusted by micrometer screws with an accuracy of 0,01 mm in both directions, and the angle of incidence and reflection are kept constant within $0,01^{\circ}$.

Absolute reflectivity of the "microsamples" can be measured by comparing the reflected light intensities detected with the light beam focussed on the semple S and reference surface R, respectively. Absolute reflectivity of the reference surface R is determined in the "reflectometer-operation" of the arrangement, as described above.

The sample holder is shown in figure 3. Its construction enables transmission measurements of semitransparent crystals and thin layers. The reflectivity of the same small area may be determined simultaneously.

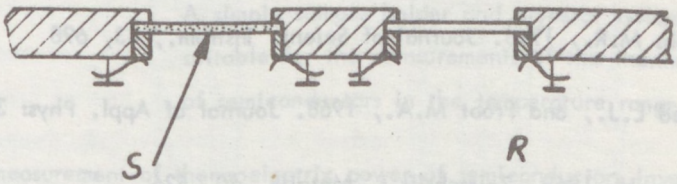

Fig. 3. Diagram of the sample holder: S - sample, R - reference mirror

3. Conclusions. Applications

By using mirrors and special reflection objectives with MgF_2 coated metallic surfaces and other detectors instead of the photomulitpliers the same reflectometer-microreflectometer arrangemat can be employed in the vacuum ultraviolet and in the near infrared spectral ranges without significant modifications.

Fig. 4 shows the reflectivity spectrum of a small size a 2 mm x 3 mm GaP-ZnS mixed crystal measured on an 0,2x0,5 mm area.

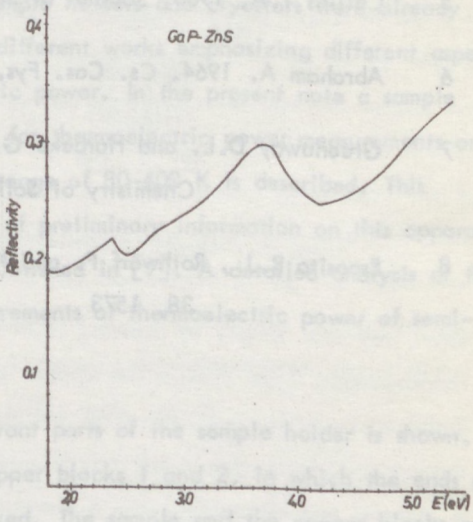

Fig.4 Reflectivity of a GaP-ZnS mixed crystal (composition: 50 mole % GaP, 50 mole % ZnS, measured on an 0,2 mm x 0,5 mm area.

The simultanous measurement of transmission and reflectivity of very small crystal areas or thin films has many applications: e.g. the investigation of uniformity of the thickness of semiconductor wafers, the determination of the optical constants and the thickness of thin dielectric or metallic films.

References

1 Wolken J.J., Forsberg R., Gallik G., and Florida R. 1968 Rev. Scient, Instrum: 39, 1734

2 Tubbs M.R., 1966. Journal of Scient. Instrum., 43, 698

3 Fried L.J., and Froot M.A., 1968. Journal of Appl. Phys: 39, 5732.

4 Knosp H. 1969. Zeitschrift f. Metallk. 60, 526

5 Collins T.A. 1966. Journal of Scient. Instrum., 44, 65

6 Abraham A. 1964. Cs. Cas. Fys., 14, 24

7 Greenaway D.L. and Harbeke G., 1965. Journ. of Physics and Chemistry of Solids, 26, 1958

8 Esposito R.J., Rothwarf F. and Kozul S., 1967. Rev. Scient. Instrum., 38, 1573

AN APPARATUS FOR THERMOELECTRIC POWER MEASUREMENTS ON SEMICONDUCTORS

K. Somogyi and B. Pődör

Abstract

A simple sample holder and cryostat system is described, suitable for the measurements of the thermoelectric power of semiconductors in the temperature range of 80–400 K.

The measurement of thermoelectrix power of semiconductors involves many well-known experimental difficulties, though in principle the measurement is quite simple. Several designs of sample holders and cryostats were already discribed in the literature [1-6], different works emphasizing different aspects of the measurement of thermoelectric power. In the present note a sample holder and cryostat system suitable for thermoelectric power measurements on semiconductors in the temperature range of 80–400 K is described. This communication serves as a medium of preliminary information on this apparatus the description of which will be published in [7]. A detailed analysis of the problems connected with the measurements of thermoelectric power of semiconductors can be found in [8].

In Fig. 1. the outline of the relevant parts of the sample holder is shown. Its most important parts are the copper blocks 1 and 2, in which the ends of the prism shaped sample can be fixed. The sample and the copper blocks are surrounded by the vapours of boiling liquid nitrogen. Each of them is fitted with a T-shaped movable piece 3, fixed by brass screws 4 and springs 5. The ends of the sample 6 are to be attached between the copper blocks and its T-shaped parts. Experience showed later that the sample can be mounted in an

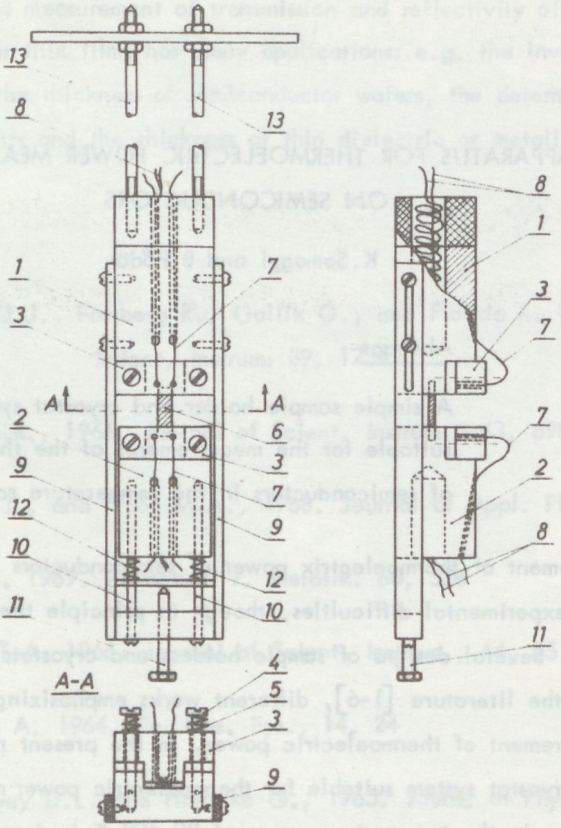

Fig. 1. Schematic outline of the sample holder (see text)

other way too, simply by pressing it in between the two copper blocks. The thermocouples 7 go through the copper blocks, then through a hole into the T-shaped movable parts, touching the samples. In this way the heat conduction through the thermocouple wires is minimized. The material of the thermocouples is chromel and alumel, having a diameter of 0.4 mm, therefore the effects of possible inhomogeneities in the thermocouple wires are eliminated [4]. The ends of the thermocouples are soldered to the movable parts of the sample holder.

The copper blocks are heated by heaters 8 placed inside the blocks. In this way the heat transfer to the surrounding medium takes place through the sample blocks, minimizing both the heat transfer to the nitrogen gas and the convection of the latter. Moreover, the maximum temperature of the surrounding medium does not exceed the temperature of the copper blocks.

The two copper blocks are connected by textile-bakelite rods 9 and brass rods 10 in such a way that with the help of screw 11 the distance between them can be varied, while the spring 12 assures the elastic connection between the copper blocks. The ends of the sample can be clamped between the movable and fixed parts of the copper blocks, or if necessary they can be simply pressed between the copper blocks. Those parts of the sample holder which make direct contact with the sample are covered by a 20-30 μm thick gold foil to ensure good electrical and thermal contacts as well. The sample holder is mounted on two rods of low heat conductivity 13. The whole sample holder is placed into a thick walled (1.5-2 mm) glass tube, closed at the bottom, and the whole assambly is lowered into a Dewar containing liquid nitrogen (see Fig.2.). Liquid nitrogen is poured into the glass tube too, up to the middle of the lower copper block. In this way the sample holder and the sample are in the vapour of boiling nitrogen. Without switching on the heater of the lower block, its temperature reaches 77 K, and nearly the same temperature can be measured on the lower end of the sample. With the other heater a convenient temperature gradient can be established and maintained during the measurements, regulating simultaneously the input power of the two heaters. During the heating the liquid nitrogen of the glass tube boils off. At measurements above room temperature the outer Dewar can be filled with water.

The convection of the nitrogen gas does not influence the measurement procedure because the thermocouples partly go through the copper blocks [2,5], and on the other hand the big copper blocks ensure an effective thermal screening of the sample.

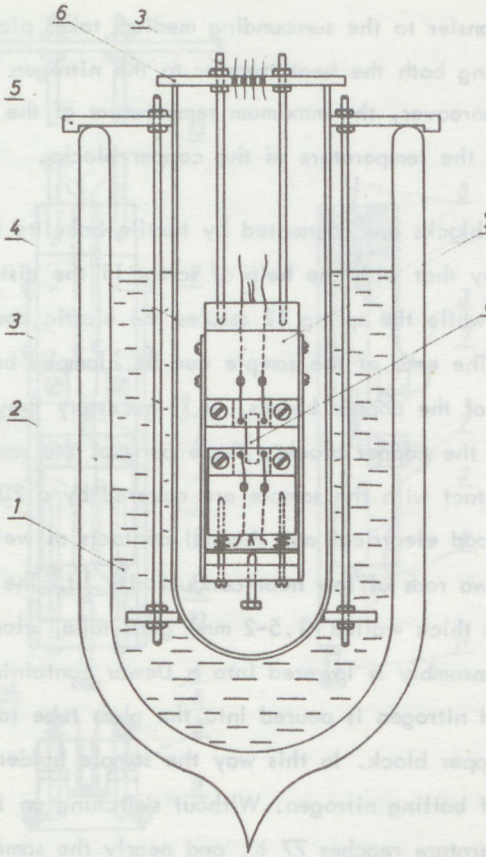

Fig. 2. The Dewar system. 1 - liquid nitrogen, 2 - Dewar, 3 - support rods, 4 - glass tube, 5 - top of the Dewar, 6 - top of the sample holder, 7 - sample holder blocks, 8 - sample.

The temperature gradient on the sample can be varied between wide limits. According to our experiences the most suitable temperature gradient was 5-10 K. In this case the lowest limit of the measurements was about 80-85 K (the average temperature of the sample). The upper temperature limit is determined by the contacting material used for making electrical contacts on the sample, and in our case it was about 400 K.

The measurement of the thermoelectric voltage of the semiconductos sample was accomplished with a d.c potentiometric system or with a sensitive digital voltmeter. The termocouple voltages were measured by a potentiometer too.

We have found that the measuring apparatus is simple to work with and it is reliable, providing the contacts on the sample are ohmic or of low resistance.

The accuracy of the measurements is better than 10 per cent. Near and above room temperature it might even be better. In order to control the function of the set up we made measurements of thermoelectric power on pure Ge samples. In Fig. 3. a typical result of such a measurement on n-Ge is shown and is

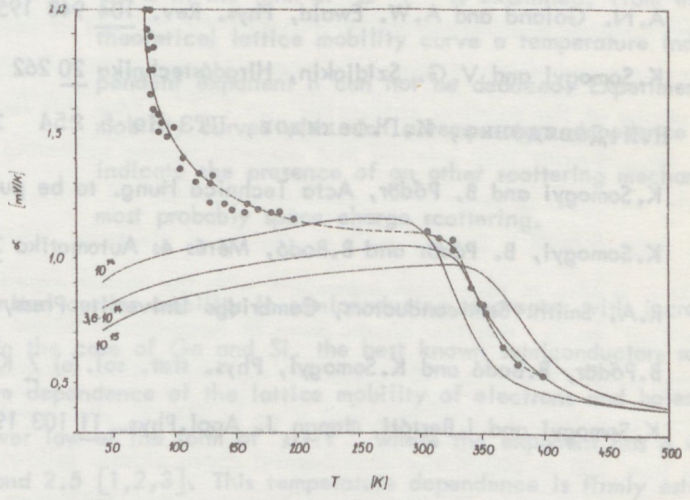

Fig. 3. Typical results on a pure n-Ge sample with a donor concentration of 3.6×10^{14} cm^{-3}. Theoretical curves are calculated without taking into account the phonon drag effect for donor concentrations of 1×10^{14}, 3.6×10^{14} and 1×10^{15} cm^{-3} respectively.

compared with the appropriate theoretical curves, without taking into account the phonong-drag effect which predominates at low temperatures. Our experimental results compare favourably with those found in the literature [9]. Near and above room temperature where the phonon drag effect is negligible the measured curve coincides with the calculated one.

Some results of thermoelectric power measurements on semiconductors obtained with the help of this apparatus are described in [10, 11].

The authors gratefully acknowledge the participation of Miss B. Bodó in setting up the apparatus and in performing some of the measurements.

References

1. T.H. Geballe and G.W. Hull, Phys. Rev. 94 1134 1954.
2. A.E. Middleton and W.W. Scanlon. Phys. Rev. 92 219 1953.
3. В.И. Фистуль, К.В.Черкас, ФТТ 4 3288 1962.
4. A.N. Goland and A.W. Ewald, Phys. Rev. 104 948 1956.
5. K.Somogyi and V.G. Szidjakin, Hiradástechnika 20 262 1969.
6. Н.И.Давиденко, И.Г.Факидов, ПТЭ Но 5 254 1967.
7. K.Somogyi and B. Pődör, Acta Technica Hung. to be published
8. K.Somogyi, B. Pődör and B.Bodó, Mérés és Automatika 21 130 1973.
9. R.A. Smith: Semiconductors, Cambridge University Press, 1959.
10. B.Pődör, B.Bodó and K.Somogyi, Phys. stat. sol.(a) 7 K105 1971.
11. K.Somogyi and I.Bertóti, Japan J. Appl.Phys. 11 103 1972.

A NOTE ON THE TEMPERATURE DEPENDENCE OF ELECTRON MOBILITY IN GaAs

B. Pődör and N. Nádor

Abstract

The possibility of describing the electron mobility of GaAs in the form of $\mu \sim T^{-n}$ is examined. From the theoretical lattice mobility curve a temperature independent exponent n can not be deduced. Experimental mobility curves with such a temperature depedence indicate the presence of an other scattering mechanism, most probably space charge scattering.

The lattice limited carrier mobility in semiconductors decreases with increasing temperature. In the case of Ge and Si, the best known semiconductors so far, the temperature dependence of the lattice mobility of electrons and holes obey an inverse power law of the form of $\mu \sim T^{-n}$ where the exponent has a value between 1.5 and 2.5 [1,2,3]. This temperature dependence is firmly established for the electrons and holes in Ge and Si in a wide temperature range and can be theoretically interpreted invoking acoustic phonon scattering with an admixture of nonpolar optical scattering, and in the case of holes in Ge (and presumably in Si too) including the effects of the valence band structure. Motivated perhaps by this success, the experimental mobility curves of the more complicated compound semiconductors were repeatedly described in the literature by inverse power law functions.

A compilation of such experimentally derived inverse power law functions for the mobility of electrons and holes in $A^{III}_{B}{}^{V}$ type compound semiconductors and in lead chalcogenides can be found in [1]. Because of the predominant role of polar optical phonon scattering in most of the compound semiconductors of $A^{III}_{B}{}^{V}$ and $A^{II}_{B}{}^{VI}$ type [4,5,6] with its characteristic exponential temperature dependence, the inverse power law in these semiconductors can not be founded theoretically. Nevertheless the description of experimental mobility curves in this form has been widely used until now.

In this note we would like to discuss some aspects of this problem as applied to the case of n-type GaAs.

Nasledov et al. [7] have measured the electron mobility of GaAs at high temperatures and observed that with increasing temperature the temperature dependence of the mobility approaches $\mu \sim T^{-3/2}$. From this fact and from other measurements they inferred that acoustic phonon scattering dominates the mobility in GaAs at least at elevated temperatures [7]. Fistul' [1] quotes $\mu = 8500\ (T/300)^{-1}$ for the lattice mobility of electrons. While the value at 300 K is also in reasonable agreement with the recent experimental and theoretical results, this law breaks down at temperatures below 300 K. As recently as in 1972 Blood [8] measured the temperature dependence of electron mobility in epitaxial GaAs from 300 K up to 800 K, and found that in the range from 300 to 500 K the experimental curve closely follows a $\mu \sim T^{-n}$ law, with n = 1.24-1.26. The slope of his experimental curves somewhat diminishes above 500 K and above 650 K it rises again, but this rise is due to the onset of conduction in the X conduction band minima. Blood has compared the slope of the experimental curve with that of the theoretical mobility curves calculated recently by Rode [9] and Rode et al. [10], and found a reasonable agreement between 300 and 400 K, the slope of the calculated curve being somewhat larger. However the experimental mobility data was about 20 per cent lower than the theoretical mobility[8]. Rode's calculated curve also showed a decrease in its slope above 500 K.

We have recently measured the temperature dependence of the electron mobility of liquid phase epitaxial GaAs, having an electron concentration in the range of 10^{15} - 10^{16} cm^{-3} [11]. Most of the experimental mobility curves if drawn in a double logarithmic scale are linear in the temperature range of 200-400 K. The corresponding exponent in $\mu \sim T^{-n}$ is n_{exp} = 1.13 - 1.26 for the different samples having a room temperature electron mobility of about 5000-6000 cm^2/Vs.

The theoretical lattice mobility was also recalculated by us [11,12,13]. Based on these calculations we have evaluated the exponent n simply by taking the logarithmic derivative of the calculated curve. The calculated values of n_{th} are shown in Fig. 1. For the sake of reference the calculated lattice mobility is shown in Fig. 2. together with its components [12,13]. According to the curve presented in Fig. 1. n_{th} shows a strong temperature dependence, even in the relatively narrow interval from 300 to 500 K referred to above. At the

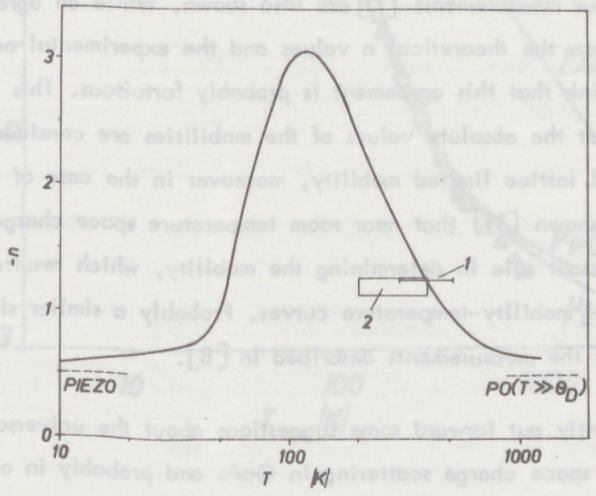

Fig. 1. The temperature dependence of the theoretical value of - n = d (ln μ) / d (ln T) for the lattice mobility of electrons in GaAs. 1 - measured by Blood [8], 2 - our measurements.

lowest temperatures ($T \lesssim 30$ K) piezoelectric scattering dominates the mobility and n_{th} approaches 0.5 the characteristic exponent in the temperature dependence

of piezoelectric mobility [6]. For $T \lesssim 50$ K neglecting polar optical phonon scattering we have $n_{th} = d\,(\ln \mu) / d\,(\ln T) = -\,(1/2 + \frac{1}{1 + \mu_{AC}/\mu_{PIEZO}})$ and with decreasing T μ_{AC}/μ_{PIEZO} increases as T^{-1}.

With increasing temperature n_{th} rises to its maximal value at about 120 K and then falls again. Above 100 K polar optical scattering dominates the mobility [12,13], and this is reflected by the strong temperature dependence of n_{th}. For temperatures $T > \Theta_D = 420$ K, the Debye temperature for longitudinal optical phonons, but below about the melting point, where the influence of acoustic phonon scattering is already considerable, n_{th} falls to about 0,6 wnick is close to the theoretical value of 0.5 for polar optical phonon scattering in the high temperature limit [2,6] (see [12,13] too).

In Fig. 1. the experimentally determined n values from the work of Blood [8] and from our measurements [11] are also shown. While an agreement can be seen between the theoretical n values and the experimental ones at about 400 K, we think that this agreement is probably fortuitous. This is based on the observation that the absolute values of the mobilities are considerably less than the theoretical lattice limited mobility, moreover in the case of our samples we have already shown [11] that near room temperature space charge scattering plays an important role in determining the mobility, which results in a decrease of the slope of mobility-temperature curves. Probably a similar situation exists in the case of the measurements described in [8].

We have recently put forward some suggestions about the universal occurrence and nature of space charge scattering in GaAs and probably in other compound semiconductors too [14]. We therefore suggest that in those cases where the experimental mobility curves csan be described with a temperature dependence of the form of $\mu \sim T^{-n}$, besides lattice scattering, space charge scattering plays an important role in determining the mobility.

The authors are deeply indebted to Dr. I. Bertóti for growing the epitaxial GaAs samples on which the measurements referred to above were performed.

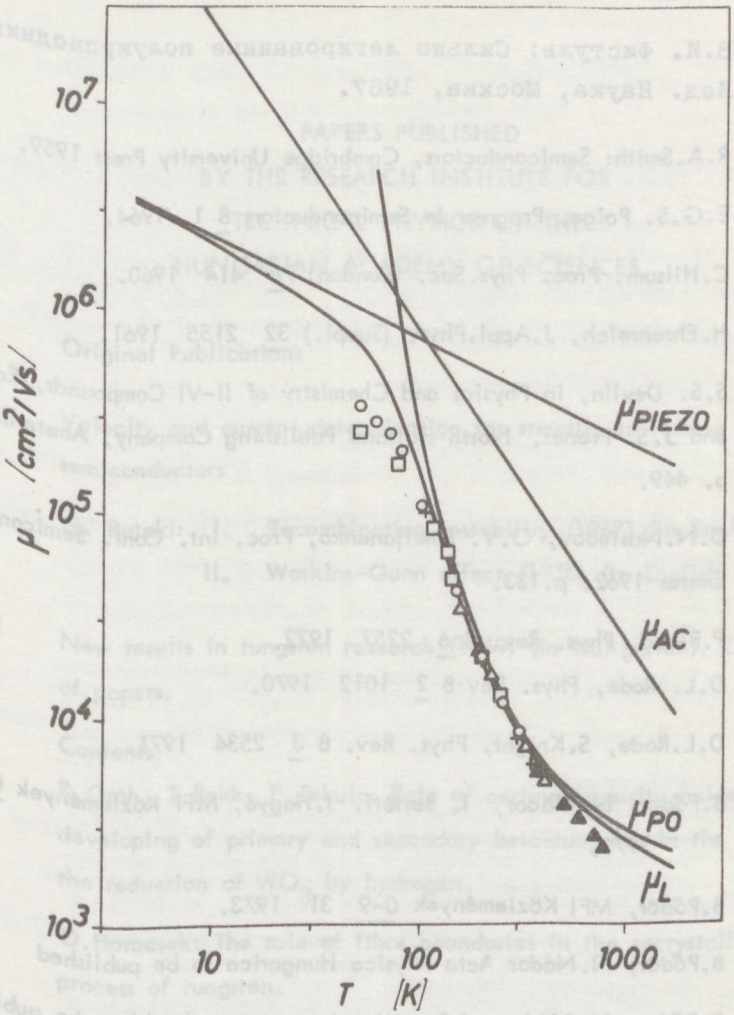

Fig. 2. The calculated lattice limited electron mobility of GaAs [11,12,13]. μ_L - lattice mobility, μ_{PO} - polar optical phonon mobility, μ_{AC} - acoustic phonon mobility , μ_{PIEZO} - piezoelectric mibility. Experimental points are the best data recently available (see [11,12,13]).

References

1. В.И. Фистуль: Сильно легированные полуирпводники, Изд. Наука, Москва, 1967.

2. R.A.Smith: Semiconductors, Cambridge University Press 1959.

3. E.G.S. Paige, Progress in Semiconductors 8 1 1964.

4. C.Hilsum, Proc. Phys.Soc. (London) 76 414 1960.

5. H.Ehrenreich, J.Appl.Phys. (Suppl.) 32 2155 1961.

6. S.S. Devlin, in Physics and Chemistry of II-VI Compounds, Ed.M.Aven and J.S. Prener, North-Holland Publishing Company, Amsterdam 1967. p. 449.

7. D.N.Nasledov, O.V. Emeljanenko, Proc. Int. Conf. Semicond. Phys. Exeter 1962. p.133.

8. P.Blood, Phys. Rev. B 6 2257 1972.

9. D.L. Rode, Phys. Rev B 2 1012 1970.

10. D.L.Rode, S.Knight, Phys. Rev. B 3 2534 1971.

11. B.Pődör, N.Nádor, I. Bertóti. J.Hagyó, MFI Közlemények 0-9 61 1973.

12. B.Pődör, MFI Közlemények 0-9 31 1973.

13. B.Pődör, N.Nádor Acta Physica Hungarica to be published

14. B.Pődör, N. Nádor, I.Bertóti, phys. stat. sol. (a) to be published

PAPERS PUBLISHED
BY THE RESEARCH INSTITUTE FOR
TECHNICAL PHYSICS OF THE
HUNGARIAN ACADEMY OF SCIENCES

0 = Original Publications

0 - 1 Velocity and current determination for steadily travelling domains in semiconductors

G. Pataki: I. Recombination instability (1967) (in English)
II. Watkins-Gunn effect (1958) (in English)

0 - 2 New results in tungsten research (1969) (in Hungarian). Collection of papers.

Contents

0 - 2 I. Szántó, L. Varga: An X-ray method for direct particle size determination by line-profiles.

L. Uray: Investigation of thermoelectric power of industrial tungsten wires.

I. Gaál: Investigation of microplasticity of tungsten by internal friction measurements.

J. Neugebauer, M. Marczinkó, G. Schlosser, J. A. Hegedüs: Thermo-condensation of WO_3 from the hydrates of 12-silicotungstic acid.

List of T. Millner's patents

List of T. Millner's publications.

0 - 3 Some problems in semiconductor research (1971) (in Hungarian with English abstracts)

Contents

Z. Bodó: Phonon-drag investigationes in semiconductors.

J. Schanda, G. Sass: On some problems of infrared spectrometry of semiconductors.

B. Pődör, S. Zsindely, E. Papp: Preparation and properties of Cr-doped semicondusting and semi-insulating GaAs single crystals.

U. M. Vanyek: Analysis of the process for production of ZnS powders for cation-type impurities.

0 - 4 Papers in the field of tungsten research (1971) (in Hungarian with English abstracts)

Contens

A. Papp: Some problems of the theory of sintering.

A. Klug: Preparation of tetragonal potassium-tungsten-bronze and some new data on its crystal structure.

0 - 4 P.Buxbaum: Chemical methods for determination of some metallic and non-metallic traces in vacuum technical tungsten metal.

G.Gerey, F.Hammer, E.Szénfy: Some observations on internal arcing phenomena in gas filled incandescent lamps.

A.Nagy: X-ray diffractometry for the study of diffusion processes.

0 - 5 Ellispsometric Tables of the Si-SiO_2 System for Mercury and HeNe Laser Spectral Lines. Ed.by G.Gergely with the co-operation of G. Forgács, B. Szücs, D.Van Phouc. Budapest, Akadémia Kiadó 1971 (in English).

0 - 6 Some Aspects of Spectrometry. By J.Schanda (1973). Electrostatic Energy in Abrupt Semiconductor Heterojunction. By I.Markó (1973). On the Minority Carrier Lifetime Anisotropy in Plastically Deformed P-Type Germanium, By I.Cseh, and B.Pődör (1973) (in English).

0 - 7 Papers in the field of tungsten research (1972) (in Hungarian)

Contents

0 - 7 T. Geszti: On thermodynamic calculations of halogen lamps.

I. Hangos - I. Juhász: Simultaneous equilibria in halogen lamps containing two different kinds of halogen atoms.

I. Hangos - T. Deutsch - B. Szücs - Gy. Gyergely: Factors influencing the stationary state of halogen lamps.

I. Hangos - A. Salamon - L. Bartha: Radio-chemical investigation of physico-chemical processes of halogen lamps. I.

I. Hangos - L. Bartha: Radio-chemical investigation of physico-chemical processes of halogen lamps. II.

0 - 8 Papers in the field of tungsten research (1973) (in Hungarian).

Contents

T. Millner: The story of the berillium containing dopant for large-crystalline tungsten metal.

T. Millner - R. Gróh: Comparative termogravimetric test of two intermediate products from the tungsten production of the TUNGSRAM works.

T. Szalay - L. Bartha: Radiotracerinvestigation of the interaction between different tungsten oxides and thallium (III) chlorid.

L. Kozma - L. Bartha: Autoradiographic investigation of the diffusion in swaged powder-metallurgical tungsten.

O. Horacsek: Formation of grain boundary cavities during high temperature creep in tungsten wires.

T. Geszti: On the description of the transport processes in halogen incandescent lamps containing carbon additives.

I. Hangos - L. Bartha: On the role of impurities evaporating from incandescent filaments in halogen lamps.

0 - 8 Gy. Gerey- I. Gaál: Halogen incandescent lamp with negative differential resistance.

T. Millner: Recent results in the field of tungsten research.

K. Vasasdi: Separation methods for analysis of the impurities in tungsten.

Gy. Gergely: Electronspectroscopy of tungsten.

B. Molnár - L. Uray - I. Gaál: Determination of the gas pressure in burning incandescent lamps.

0 - 9 Some Reports of the Scientific Staff of the Research Institute for Technical Physics of the Hungarian Academy of Sciences. (1973).

Contents

P. Liem - P. Sviszt - B. Tóth: On the calculation of activation energies from the thermoluminescence curves.

B. Pődör: Lattice scattering limited mobility of electrons in GaAs.

K. Somogyi: Contacts and sample preparation on semiconductor layers for Van Der Pauw measurements.

B. Pődör - N. Nádor - I. Bertóti - J. Hagyó: Current carrier scattering and electrical properties of liquid phase epitaxial GaAs.

K. Somogyi: Analysis of Hall data and mobilities in GaP.

J. Lánc - J. Peisner: Measuring and recording of photoemission electron energy distribution by an analog differentiator.

0 - 10 Mrs. M. Farkas - Jahnke: Determination of the structure of polytypes built up from translationally equivalent layers by a new direct method, and the application of the method for the investigation of crystals containing stacking faults. (1973) (in Hungarian with English abstract)

0 - 11 Papers in the field of new tungsten research (1974) (in Hungarian)

Contents

0 - 12 L.Gutai: Local determination of galvanometric properies in semiconductors - an application of the solution of a bundary value proglem in potential theory. (1974) (in Hungarian with English introduction and content)

R = Review articles (in Hungarian)

R - 1 I.Szántó: X-ray topography of lattice defects in solids (1968).

R - 2 L. Gutai: Measurement of the physical parameters of epitaxial semiconductor layers (1968).

R - 3 C. Székely: Formation of lattice defects in epitaxial semiconductor layers (1968).

R - 4 I. Szántó: X-ray topography of lattice defects in solids II. (1971).

Selected papers from the oeuvre of E. Winter (1967).

Selected papers from the oeuvre of T. Millner (1969).

BIBLIOGRAPHY

A comprehensive list of publications of the scientific staff of the Research Institute for Technical Physics of the Hungarian Academy of Sciences. (1972)

Collected by É. Gomperz with cooperation of Z. Bodó and G. Gergely.

(In original language of the papers, with English translations of titles.)